REPORT NO. FRA-RT-73-34

TOWING TANK TESTS ON A RAM WING IN A RECTANGULAR GUIDEWAY

Yves A. Boccadoro

JULY 1973

FINAL REPORT

Prepared for

DEPARTMENT OF TRANSPORTATION
FEDERAL RAILROAD ADMINISTRATION
Office of Research, Development and Demonstrations
Washington DC 20591

TECHNICAL REPORT STANDARD TITLE PAGE

1. Report No.	2. Government Accession No.	3. Recipient's Catalog No.
FRA-RT-73-34		

4. Title and Subtitle	5. Report Date
TOWING TANK TESTS ON A RAM WING IN A RECTANGULAR GUIDEWAY	July 1973
	6. Performing Organization Code

7. Author(s)	8. Performing Organization Report No.
Yves A. Boccadoro*	DOT-TSC-FRA-73-8

9. Performing Organization Name and Address	10. Work Unit No.
M.I.T. Aerophysics Laboratory 560 Memorial Drive Cambridge MA 02139	RR407/R4302
	11. Contract or Grant No. DOT-TSC-239
	13. Type of Report and Period Covered Final Report June 1, 1971 to October 31, 1972
12. Sponsoring Agency Name and Address Department of Transportation Federal Railroad Administration Office of Research, Develop. & Demon. Washington DC 20591	14. Sponsoring Agency Code

15. Supplementary Notes

*Under Contract to: Department of Transportation, Transportation Systems Center, Kendall Square, Cambridge MA 02142

16. Abstract

The object of this study was to set the theoretical and experimental basis for a preliminary design of a ram wing vehicle. A simplified one-dimensional mathematical model is developed in an attempt to estimate the stability derivatives of this type of vehicle. Although very basic, the approach that was taken allows for any geometry of both the model and the guideway. A survey is made of various possible testing techniques. The experimental results obtained using the towing tank technique are reported and compared with the computed estimates. Although many results are very encouraging, the limited data do not allow for a precise estimation of the validity of the mathematical model. It is concluded that the towing tank technique is adequate for the type of investigation that is required at this early stage of the design.

17. Key Words	18. Distribution Statement
Vehicle, ram-wing:test, towing-tank	DOCUMENT IS AVAILABLE TO THE PUBLIC THROUGH THE NATIONAL TECHNICAL INFORMATION SERVICE, SPRINGFIELD, VIRGINIA 22151.

19. Security Classif. (of this report)	20. Security Classif. (of this page)	21. No. of Pages	22. Price
Unclassified	Unclassified	116	

Form DOT F 1700.7 (8-69)

PREFACE

The work described in this report represents part of an ongoing effort to develop a high speed ground transportation vehicle utilizing aerodynamic forces for suspension. Small scale model demonstrations of this concept were carried out at Princeton University as early as 1965, and low level efforts have been carried out at the Massachusetts Institute of Technology and elsewhere since then. The Federal Railroad Administration has funded this program for the past four years, through the Office of Research Development, and Demonstrations.

The present report documents recent experimental results and compares them with a simplified theory. Additional theoretical efforts are summarized in a separate report. Sufficient promise has been shown by this concept to initiate a system definition study which will define the characteristics of a complete ram air cushion vehicle and guideway. It is anticipated that the results of this study will become available in the summer of 1973.

TABLE OF CONTENTS

LIST OF ILLUSTRATIONS

LIST OF ILLUSTRATIONS (continued)

SYMBOLS

A	area beneath the model
AR	aspect ratio = $\frac{b}{c}$
b	width or span of model
B	angle of tapered sides
c	length or chord of model
$C_{(...)}$	nondimensional coefficient, e.g. $Cp=\frac{p-p_\infty}{1/2\rho U^2}$
G	center of resolution
$\hat{G} = \frac{G}{b/2}$	nondimensional center of resolution
h	ground clearance
$\hat{h} = \frac{h}{c}$	nondimensional ground clearance
i_A, i_B, etc. ...	nondimensional moments and products of inertia
ℓ	rolling moment
ℓ_1	height of vehicle
L	lift
L, M, N	moments about x,y,z (Appendices only)
m	mass of model
p	pressure
p, q, r	angular velocities about x,y,z
R	width of vehicle lip
Re	Reynolds number
$q = 1/2\rho U^2$	dynamic pressure
U, V, W	linear velocities about x,y,z
U_a	spanwise constant approximation of U

SYMBOLS (continued)

X_o	midchord point
Y	side force
α	angle of attack
β	side slip angle
ε	ground clearance
$\hat{\varepsilon} = \frac{\varepsilon}{c}$	nondimensional ground clearance
ψ	yaw angle
δ	side displacement
$\hat{\delta} = \frac{\delta}{b/2}$	nondimensional side displacement
δ_o	side gap
ν	kinematic viscosity
ρ	fluid density
$\mu = \frac{m}{\rho U_\infty{}^2 S}$	nondimensional mass
ϕ	roll angle
θ	pitch angle
$(...)'$	differentiation with respect to X
$(...)_{TE}$	value at trailing edge
$(...)_\infty$	free stream value
$(...)_{\alpha,\delta,\phi...}$	derivative with respect to the variable used as subscript

Chapter 1

INTRODUCTION

The term "ram wing", which is used in this report, refers to a ground effect vehicle which uses pure aerodynamic lift for suspension. The term initially was developed to differentiate such a ground vehicle from one which used a pressurized air cushion for suspension. Recently, (ref. 23) more precise terminology has appeared. A ground vehicle suspended by aerodynamic lift only is called a "dynamic ram air cushion" vehicle. The flow beneath the vehicle is allowed to exit freely at the trailing edge, and a forward velocity is needed to develop a lifting pressure beneath the vehicle. Present air cushion designs use a compressor to energize the fluid, which is contained beneath the vehicle by some type of partial barrier to maintain an elevated pressure. No forward velocity is needed for suspension. In this report, the term "ram wing" is used to describe a "dynamic ram air cushion vehicle."

In addition to making use of ground effect to improve the lift to drag ratio at high velocities, the ram-wing vehicles also use side-wall effects for their lateral stability. In this report we restricted ourselves to open air type vehicles as opposed to enclosed tube type vehicles. The concept of the ram wing as a high speed (typically from 300 to 500 miles per hour) ground transportation system is very recent and little

literature is available on the subject. Some experiments (such as the glide test of ref 1) have already demonstrated the feasibility of the concept itself. The next step in designing a practical vehicle is to optimize the cross section of the vehicle and guideway. This can be done only if both experimental data and theoretical estimates of the aerodynamic performance and the stability characteristics of the vehicle are available. Therefore the object of the present study was to set the basis for a first order modeling of these vehicles and to define an adequate testing technique.

A simplified mathematical model that can be used to estimate the stability derivatives of various geometric configurations of the ram wing can be found in this report. After a more general description of the flow it was found that a one-dimensional approximation with "leakage" similar to that used by Gallington, in ref 2, could be used when the vehicle is fitted with side lips reducing the side clearance to a quantity as small as allowed by construction considerations. Because of the very specific problems involved in testing a ground effect machine, a survey of the available testing techniques was completed. It is concluded that no single facility is available that would yield all the information that is required to design a new means of transportation. The towing tank was finally chosen since it was felt that the urge was for a testing technique that was cheap, readily available, and would give the stability derivatives of a given vehicle as opposed to its detailed flow configuration.

The results from two series of experiments are reported here and are compared with the computed estimates.

Chapter 2

A MATHEMATICAL MODEL TO ESTIMATE SOME STABILITY DERIVATIVES

2.1. Introduction

The dynamics of a Ram Wing vehicle in a trough differ strongly from those of a traditional aircraft in that the derivatives of the forces and moments caused by displacements (as against velocities) not only are not negligible but are the most important. The derivation of the linearized lateral equations of motion pertinent to the kind of vehicle we are dealing with can be found in Appendix A. It is seen that the undamped frequencies depend solely on these "static" stability derivatives. The damping will obviously depend on the dynamic derivatives (i.e. those caused by velocities), but as seen in the development of Appendix C, additional damping can easily be obtained by a simple control system. The purpose of this chapter is therefore to find a method to estimate these static derivatives for various ram wing configurations.

Barrows (refs. 1 and 3) has analyzed the flow around several configurations of ram wing vehicles using the asymptotic expansion method. However, this method requires some assumptions concerning the order of magnitude of the various important parameters involved and also becomes rapidly complicated with increased complexity of the geometry.

Gallington et al. (ref 2) following the work of Kaario (ref 4) and Lippisch (ref 5) has used a very simplified one dimensional flow analysis which yields good experimental matching with his simple model. The great advantage of this method is its flexibility to take into account any geometry with minor changes to the analytical derivations. Coupled with its simplicity this makes it the logical choice for comparison with our experiments here. It should be added that the thickness effects and the pressure field above the vehicle will be neglected as it was demonstrated (ref 3) that their influence is small compared to the contraction effect below the vehicle.

2.2. General Formulation for Symmetric Model and Attitude

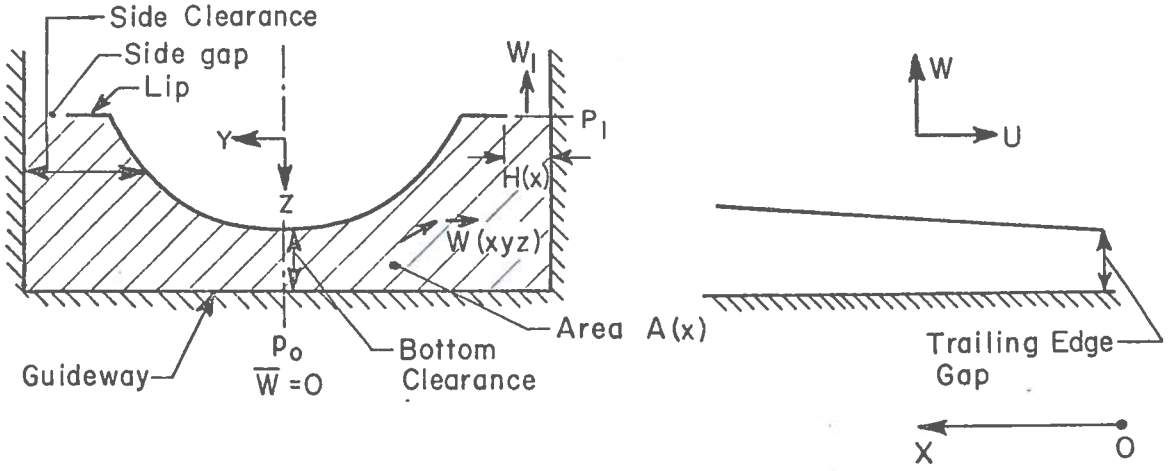

Let us consider a model and a guideway of arbitrary cross sections, but symmetric, as sketched above.

Let us define the following notation:

$\vec{W}$ is the local velocity vector in the y-z plane.

W is its magnitude nondimensionalized by U_∞.

U is the nondimensional forward velocity.

The index $_0$ is used to indicate values in the x-z plane.

The index $_1$ is used to indicate values just past the side edge of the model

$$C_p = \frac{p - p_\infty}{1/2\rho U_\infty^2}$$

x nondimensional chordwise position (varies between 0 and 1). Origin at trailing edge.

Mass conservation will give us our basic equation. It states that the mass coming in the channel region under the model must come out either through the trailing edge or through the side gap.

Since the mass escaping through the side gap varies with chordwise position we must integrate along c. When written for an arbitrary section at a distance x from the trailing edge this becomes

$$2c \int_x^1 W_1(x)\, H(x)\, dx + \iint_A U(x,y,z)\, dy\, dz = \text{const}$$

Let $U_a(x)$ be the average forward velocity in the cross section

$$\iint_A U(x,y,z)\, dy\, dz = U_a(x)\, A(x)$$

and the mass conservation becomes

$$2c \int_x^1 W_1(x)\, H(x)\, dx + U_a(x)\, A(x) = \text{const}$$

Taking the derivative with respect to x and using the non-dimensional terms

$$\hat{A} = \frac{A}{c^2} \qquad \hat{H} = \frac{H}{c}$$ we obtain

$$U'_a(x) = \frac{2W_1\hat{H} - U_a(x)\ \hat{A}'}{\hat{A}}$$

If W_1 could be related to $U_a(x)$ this equation would yield a solution for $U_a(x)$.

We shall first assume that the Bernoulli equation holds along a streamline yielding:

$$C_p(x,y,z) = 1 - W^2(x,y,z) - U^2(x,y,z)$$

and in particular at the side gap

$$C_{p_1} = 1 - W_1^2(x) - U_1^2(x)$$

To carry on simply an assumption must be made on the value of p_1 or C_{p_1}. Unless experimental data are available it is probably good enough to assume that p_1 is equal to the free stream value or $C_{p_1} = 0$. This yields

$$W_1^2 = 1 - U_1^2$$

Again the lack of experimental data does not allow one to estimate the relation between U_1 and U_a and more generally between $U(x,y,z)$ and $U_a(x)$.

A major assumption will be made here, i.e.

$U(x,y,z)$ is constant in a section and equals $U_a(x)$

This assumption is certainly realistic enough when the configuration is close to the "leaking" model of ref 2.

With this assumption we obtain our governing equation:

$$U'(x) = \frac{\sqrt{1-U^2(x)}\ \hat{H} - U(x)\ \hat{A}'}{\hat{A}}$$

This nonlinear differential equation can easily be solved on a computer using a straight step-by-step method starting at the trailing edge with the boundary condition $U_{TE} = U_\infty$ or any other value if experimentally available. This equation is quite general and can be applied to any cross-sectional geometry. The calculation of the pressure on the axis is straightforward since $w(x,o,z) = 0$ for symmetric models yielding

$$C_{p_o}(x) = 1 - U^2$$

However, to obtain the complete pressure solution the geometry must be considered in more detail. The simplest case is that of a model with a very small side gap compared to the other dimensions of the considered area under the model. In this case the pressure can be considered constant.

In conclusion, it is seen that the flow around a model with very small side clearance can be simply described by a one-dimensional flow derivation similar to that used by Gallington in ref 2 (constant pressure and velocity in a cross section). It should be noted that the assumption of a small side clearance is not at all arbitrary. Barrows shows in ref 1 that the lift drops dramatically with increasing side clearance and so does the lateral stiffness. Therefore a small side clearance is required to obtain good aerodynamic performance and good lateral stability.

2.3. Nonsymmetric attitudes

When the model takes a nonsymmetric attitude such as roll angle, side displacement or yaw, the assumption of constant pressure under the entire model obviously does not apply any more since the interest is in pressure differences between the left and right sides. Moreover, the same governing equation cannot be used since the area A(x) does not appear to change when the model is, for example, at a roll angle.

The simplest approach to this problem is to consider the two sides separately. Let us consider, for example, a small roll angle ϕ

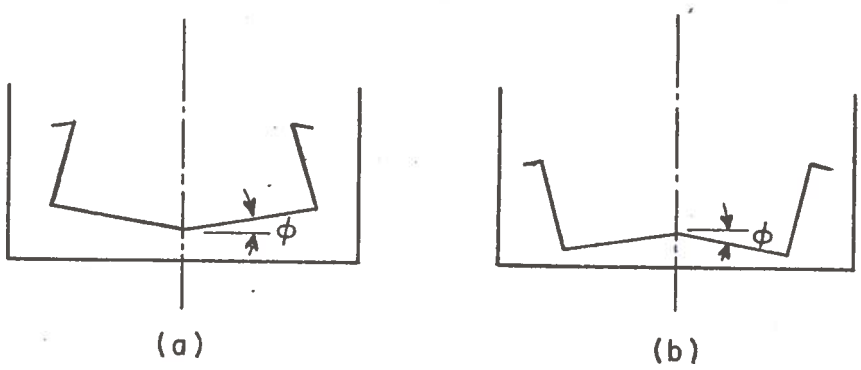

It will be assumed that the right side of the model sees the same flow as the right side of model (a) and the left side the same as the left side of model (b).

If a small enough angle is considered, the total deviation from equilibrium will be twice that of the half model (a). Then to compute, for example, the side force due to roll, we first compute the side force on half the model in the reference

position, the side force on half model (a), and take twice the difference between them.

2.4. Discussion of the Assumptions

The two major assumptions of constant forward velocity and constant pressure in a cross section have already been discussed. This section is concerned with the more minor assumptions that could easily be removed.

It was assumed that the pressure at the side gap and at the trailing edge were both equal to the free stream value, whereas the flow would more realistically look as follows:

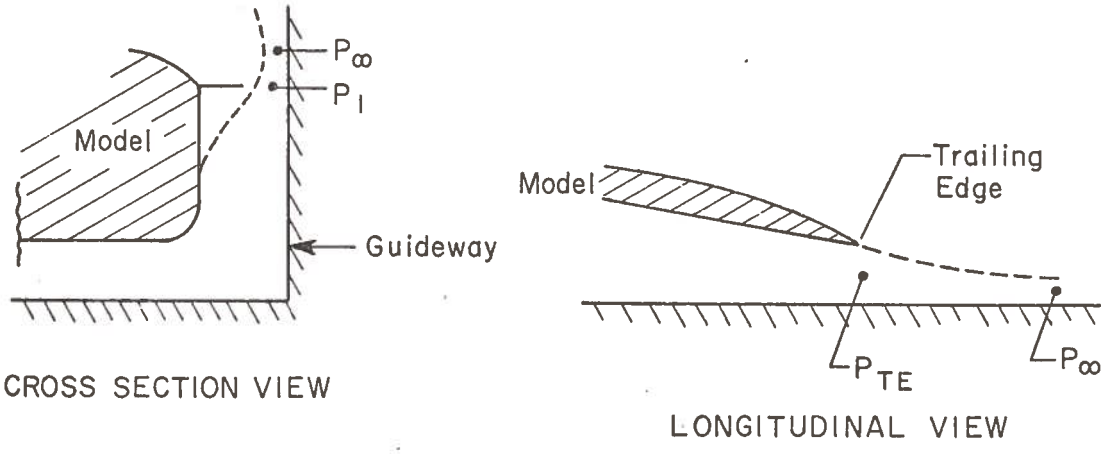

The contractions can be computed by more local and detailed analysis or determined experimentally. Before this is done some improvements could be brought in by assuming a contraction ratio at the side gap of 0.8 (cf Barrows ref 1) and using a fictitious side clearance of 0.8 the physical clearance.

Similarly when the boundary layers at the bottom or at the sides have been computed or measured, they can be included as an increase in angle of attack or in angle of side walls.

The scheme used for nonsymmetric attitudes yields a pressure discontinuity at the center. This can be removed by assuming a rounded distribution of pressure under the body.

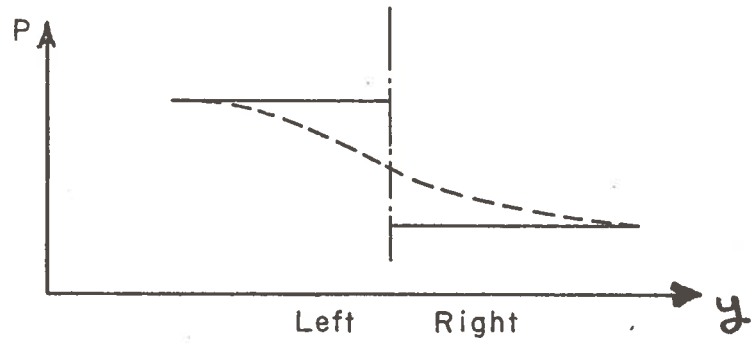

However, it should be noted that this pressure discontinuity corresponds to a model with a keel along its centerline separating the flow on the right side from that of the left side. It is very possible that this feature might be included in the design of a ram wing since it improves its lateral stability characteristics.

Finally the Bernoulli equation could be replaced by a generalized equation including a loss term.

These sophistications are not considered worthwhile at this early stage of the study.

2.5. A Detailed Solution

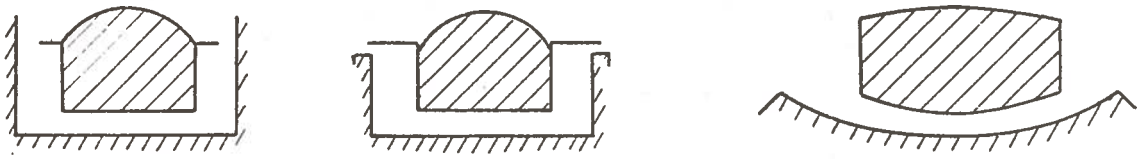

(1) (2) (3)

The same governing equation of page 7 is used for all models. A detailed computation relevant to model (1) is derived here, which also applies to model (2) with minor modifications. A derivation for model (3) can be found in ref 22.

The following symbols are used in this section:

$\frac{h_1}{c} = \hat{\varepsilon}$ nondimensional trailing edge clearance

α angle of attack

$\hat{\ell}_1 = \frac{\ell_1}{b/2}$ nondimensional height of model

$\hat{\delta}_o = \frac{\delta_o}{b/2}$ nondimensional side gap

$\hat{\delta} = \frac{\delta}{b/2}$ variation of side gap (side displacement)

ϕ roll angle

ψ yaw angle

R = lip here R = B·x; B = angle of tapered sides

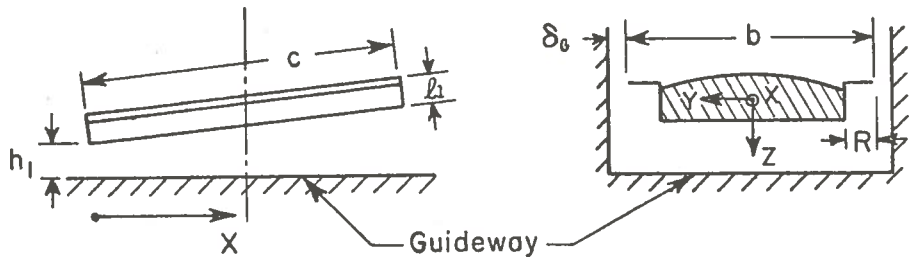

All the moments will be computed with respect to an arbitrary point called "center of resolution." It will be located at a height $\hat{G}(\hat{G} = \frac{G}{b/2})$ above the model bottom surface and at a nondimensional distance from the trailing edge of X_o.

When the model has a symmetric attitude the side clearance and the area under the model can easily be evaluated as

$$\frac{\hat{H}}{AR} = 1/2\ \hat{\delta}_o$$

$$\frac{\hat{A}}{AR} = (\hat{\varepsilon} + \alpha x)\ (1 + \hat{\delta}_o) + 1/2\ AR \cdot \hat{\ell}_1 \cdot \hat{\delta}_o + B \cdot \hat{\ell}_1 \cdot x$$

$$\frac{\hat{A}'}{AR} = \alpha(1 + \hat{\delta}_o) + B \cdot \hat{\ell}_1$$

To compute these quantities when the model is, for example, at a roll angle, they are evaluated for one-half of the model then multiplied by 2. Since only very small variations of the position with respect to the symmetric attitude are considered, the total change in area is assumed to be the sum of the changes caused by roll, yaw and side displacement.

The following expressions result, where it should be noted that $\hat{\ell}_1$ and $\hat{\delta}_o$ can be a function of x; in this case some modifications of $\hat{A}'$ are necessary.

$$\frac{\hat{H}}{AR} = 1/2\hat{\delta}_o + 1/2\hat{\delta} + 1/2\hat{\ell}_1 \cdot \phi + (x-xo)\frac{\phi}{AR}$$

$$\frac{\hat{A}}{AR} = (\varepsilon + \alpha x)(1 + \hat{\delta}_o) + 1/2AR \cdot \hat{\ell}_1 \cdot \hat{\delta}_o + B \cdot \hat{\ell}_1 \cdot x$$
$$+ 1/2AR \cdot \hat{\ell}_1 \cdot \hat{\delta} + \hat{\ell}_1 (x-x_o)\psi - 1/2AR\ \hat{\ell}_1 \cdot \hat{G} \cdot \hat{\phi}$$
$$+ \phi[AR(1/2 + \hat{\delta}_o) - 1/2Bx + \frac{Bx^2}{AR}]$$

$$\frac{\hat{A}'}{AR} = \alpha(1 + \hat{\delta}_o) + B \cdot \hat{\ell}_1 + \hat{\ell}_1\psi + \phi[-1/2B + \frac{2B}{AR}]$$

A numerical solution for U(x) can easily be obtained using a step-by-step method starting at the trailing edge with U = 1. The pressure is then obtained by

$$C_p(x) = 1 - U^2(x)$$

and the lift and pitch coefficients by

$$C_L = \int_0^1 C_p\, dx$$

$$C_m = \int_0^1 (x-x_o)\, C_p\, dx$$

The pressure distribution along the chord of the model used for the experiment computed this way for both $\phi = 0$ and $\phi = 3°$ is shown in Fig. 19.

2.6. Estimate of the Derivatives

Only the rolling moment due to roll is considered here as an example. The remaining stability derivatives are derived in some detail in Appendix B.

A rolling moment is caused by both changes in pressure at the bottom of the vehicle (independent of the position of CG)

and at the sides (dependent upon the position of CG).

The elementary rolling moment applied to a length of half model dx is

$$d\ell = C_p \frac{b}{2} \frac{b}{4} c\, dx + C_p\, c\, \ell_1 (\frac{\ell}{2}_1 - G)\, dx$$

$$\ell = \int_0^1 d\ell = \frac{b^2}{8}\, c \cdot C_L + c \int \ell_1 (\frac{\ell}{2}_1 - G)\, C_p\, dx$$

and for a model with constant height

$$\ell = \frac{b^2 c}{8} \cdot C_L + c\, \ell_1 (\frac{\ell}{2}_1 - G)\, C_L$$

$$C_{\ell_\phi} = 2\, \frac{L(\phi) - L(o)}{b^2\, c\, \phi} = 1/4[1 + \hat{\ell}_1 (\hat{\ell}_1 - 2\hat{G})]\, \frac{C_\ell(\phi) - C_\ell(0)}{\phi}$$

2.7. Summary and Conclusion

In the case when the side clearance of the model is very small compared to the other dimensions of the cross section the method developed in this chapter can be summarized as follows: the pressure and forward velocity are both assumed uniform in one cross section. The governing equation is a statement of the mass conservation combined with Bernoulli's equation and an assumption on the pressure at both the side gap and the trailing edge. This equation yields a solution for the forward velocity and the pressure as a function of the chordwise location. This enables one to compute the lift, pitching moment and momentum drag of the model for symmetric attitudes. For unsymmetric attitudes the two sides of the model are considered separately which yields a pressure discontinuity across the axis of symmetry. The lateral static stability derivatives are computed by considering the forces that result from the pressure

difference between the left and right sides of the model.

It was not expected that these simple expressions would give precise values for the stability coefficients. However, it is hoped that they can be used to determine how these coefficients vary with changes in parameters (position or geometry). For that matter this approach is interesting because no approximation on the relative magnitude of the different terms (namely angle of attack and bottom clearance) is required beforehand. Also all parameters can be taken into account. We limited outselves to the position parameters α, ε, δ, ψ, ϕ, and the geometry paramaters R, B, ℓ_1, h, AR, but the expressions could easily be modified to include curved bottom, curved sides, more sophisticated lips, etc. Thickness effects may also be included.

Chapter 3

SURVEY OF VARIOUS TESTING TECHNIQUES

3.1 General

In planning any experiment for the purpose of evaluating a high speed ground transportation vehicle, one key element must always be present. Namely, far from the vehicle the test medium is at rest with respect to the guideway, tunnel, ground or surface, while there is a relative velocity between the vehicle and the medium. This element complicates the testing procedure greatly. In addition to the constraints introduced by multiple boundaries, the usual requirements of holding Mach number and Reynolds number constant must be considered.

If the Mach number is not a serious problem, which may be the case for speeds up to 300 mph, then the Reynolds number must be considered in detail. The Reynolds number is Vl/ν, ν = the kinematic viscosity. The ratio of ν for selected fluids to ν_{AIR} is listed below:

	Glycerine	Olive Oil	Ethyl Alcohol	Water	Carbon Tetra-chloride	Mercury
$\frac{\nu}{\nu_{AIR}}$	185	7.45	0.117	0.0785	0.0448	0.00828

In spite of this range of available choices, it turns out that in practice it is very hard to simulate Reynolds number. Since we would like to test small scale models, those fluids where the ratio is greater than unity are ruled out. Note a 1/100 scale model in mercury at about full scale speeds would be at a full scale Reynolds number. At the same time since the dynamic pressure is roughly 1.1×10^4 times greater the model has the same loads as the full scale vehicle which means that the same power is required for the test as for the full scale object! Consequently a smaller Reynolds number must in general be accepted, but care must be taken to do what one can about scaling the boundary layer transition to turbulence and separation.

3.2 Possible Testing Techniques

For any fluid medium the major possible choices are:

medium	: fixed or moving
guideway	: present or simulated
means of suspension	: free fixed carriage
path	: straight or curved
propulsion	: on board catapult

For obvious reasons all combinations do not make sense. Also, because the Reynolds number would not be significantly different and because water tunnels are far less available than wind tunnels there does not seem to be a strong immediate justification for choosing water (or other liquid) instead of air. However, this is not true when considering towing

techniques, for which the use of water usually simplifies the setup. On balance, it seems that the seven schemes of Table I are the most practical ones.

TABLE I

SCHEME	COMMENTS
A. In Water	
1. Moving vehicle - straight guideway - carriage	Towing technique referred to as "Towing Tank" (cf ref 6)
B. In Air	
2. Moving vehicle - straight guideway - carriage	Towing technique. If used in conjunction with a magnetic suspension system it is good for tube vehicles.
3. Moving vehicle - curved guideway - carriage	Some interference problems (cf ref 11 to 14). Referred to as "whirling arm."
4. Moving vehicle - straight guideway - catapulted model	These are flight tests of the model.
5. Moving vehicle - straight guideway - self-powered model	
6. Moving medium - moving guideway - fixed model	Conventional wind tunnel with moving walls. Referred to as "moving belt" technique (cf ref 7 to 10).
7. Moving medium - simulated guideway - fixed model	Conventional wind tunnel with fixed images (cf ref 15).

The remaining alternatives probably have their proponents but will not be discussed here. The remainder of this chapter consists of a more detailed discussion of these seven schemes.

3.2.1. Towing techniques

All the towing techniques have in common the fact that forces and moments can easily be measured using strain gage balances. The difficulty involved in designing such balances would depend on the chosen configuration. As for the wind tunnel techniques a question is raised concerning the importance of the struts interference. An additional difficulty is to determine with accuracy the position of the model inside the guideway. Non-contact linear displacement transducers can be used if a continuous measurement of position is required. If the position only needs to be determined once when the model is at rest, a cathotometer can be used as described in ref. 15. A distance could be obtained this way with a precision of 5 mils.

Towing tank. This facility is commonly used by naval architects and marine engineers. The guideway is submerged beneath the water. The model is connected to a towing carriage out of the water by a suitable strut. The depth of the water is selected to be large enough that the surface waves are negligible. It may be possible to consider having the guideway either at the bottom of the tank or upside down near the surface of the water. In either case the maximum velocities will probably be of the order of 5 feet/second. The strong attraction of this testing scheme lies in its realistic geometry, and in the experience others have gained using towing tanks.

Towing test in air. Here high speed systems have been built. In fact, rocket-powered sleds have been run on tracks at supersonic speeds. One possibility is sketched below:

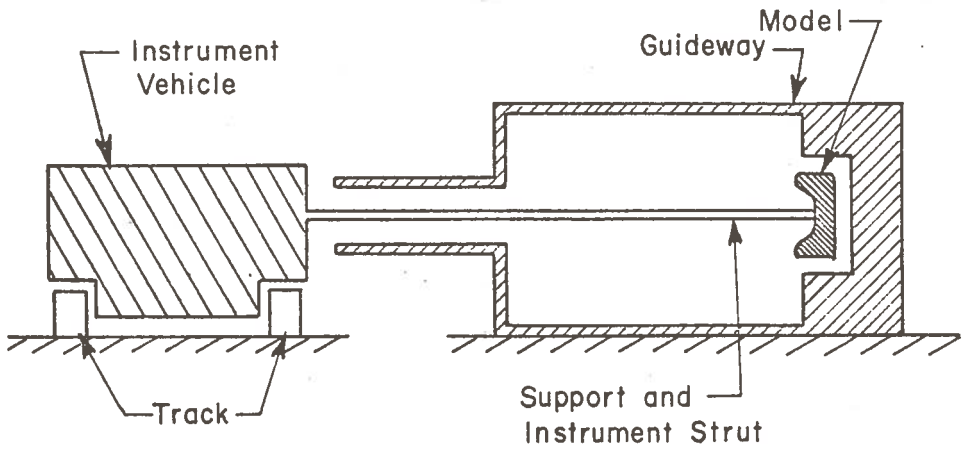

Because of the expense involved it is desirable to use an existing track. Note this system could provide full-scale speeds with 1/50 to 1/100 scale models and hence about 1/50 to 1/100 scale Reynolds numbers. This alternative should be pursued further.

Whirling arm. This towing technique uses a circular guideway. The geometry is a little complicated because the model must be curved. The speed range up to 500 feet/second is well within the state of the art although a 50-foot radius arm will experience up to 150 g's of radial acceleration. This suggests a light weight model is desirable. It may be difficult to measure side force and yawing moment accurately unless the model and guideway be rolled 90°. Perhaps two test runs will be required. The scheme is continuous in

operation and occupies a small space compared with the towing tests. Note some care must be taken to keep the air from rotating since the device will have some drag as it moves around the guideway.

The instrumentation problems (measurement of forces or position) are similar to those discussed above in the section on towed models.

Some details of a possible design for the whirling arm can be found in references 11 to 14. The main problems reported there are the following:

- A non-uniform flow in the channel and in particular the presence of a whirl and a cross flow.
- The variation in floor alignment was ±1/8-inch.
- The data have to be processed through a slip ring creating noise problems.
- The importance of a large load due to the centrifugal forces makes the design of the balances more difficult.

It is to be noted that in the above references the length of the model was very short compared to the radius of the arm and therefore did not require curvature. For our purpose the model would have to be curved, raising another question on the accuracy of the method.

It should be noted here that a whirling arm in water is also a very feasible scheme. Since a slower speed would be necessary, some of the problems mentioned above would be simplified. This scheme was not considered separately since most

of the comments on the whirling arm in air are applicable to its counterpart in water, and since the problems related to underwater operations are considered with the towing tank.

3.2.2. Free flight

Catapulted model. This test scheme is based upon use of a vehicle which glides with constant velocity on an inclined guideway. This is an easy, quick, cheap, experimental test scheme for demonstration purposes. Data extraction is difficult, unless the model scale is relatively large. Then it ceases being cheap and easy.

As far as instrumentation is concerned the main restrictions are the weight, the limitation to non-contact measurement systems, and the fact that no power is available on board. One feasible solution to obtain a continuous measurement of the position would be to use capacitance transducers. It can be shown that a pair of capacitors can be used to measure one distance with little angle interference and no necessary outside wiring. The following view from the top of the model shows the transducers necessary to get height and roll. A similar setting on the sides could give yaw and side position.

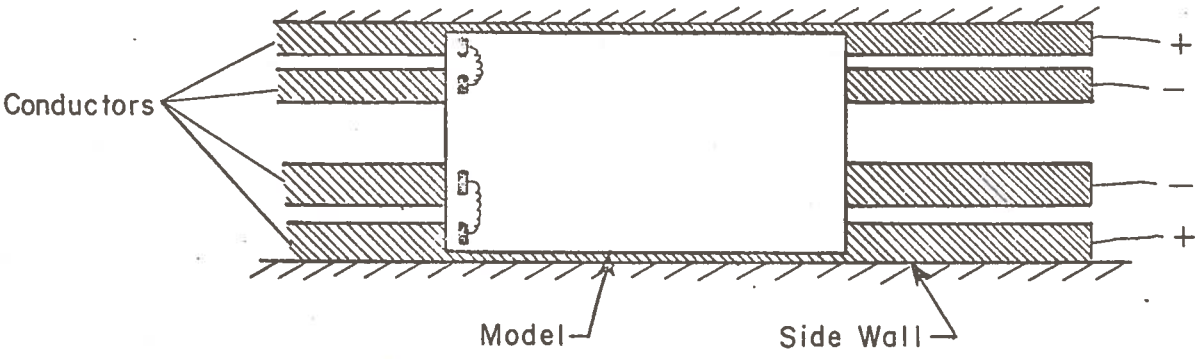

If the velocity also needs to be measured continuously this could be done using the Doppler effect.

Some preliminary experiments have been conducted (ref.1) Velocity,height, pitch and roll can be obtained with reasonable accuracy at three locations along the track. If this instrumentation might not allow one to perform a stability analysis, nevertheless it could be used to get some useful information.

The use of high speed film or stroboscopic photography can give a true picture of the behavior of the model in flight. Some ideas of the relative amplitudes and frequencies of the different motions can be deduced.

A preliminary study of the effect of geometry, clearances, control surface position and size can be conducted. For each configuration the performance (L/D) and an estimate of roll and roll rates as well as roll frequency can be obtained. An estimate of the importance of some nonlinear effects, particularly the interference between height and roll, could be deduced by measuring the roll resulting from various inputs in height (such as steps up or down, or sinusoidal ground). The influence of pitch and height on the lift coefficient C_L could be obtained by changing the weight of the model, its speed or its center of gravity.

Self-propelled model. Depending upon scale, this could be the full-size vehicle. In this case on-board instrumentation is simple. Probably the crossover between practical and and impractical, at least from the standpoint of instrumentation,

lies in the storage volume of 4 - 6 cubic feet for the transducers and for the on-board recorders. It is likely that this scheme would be most useful in the development stage between feasibility and the demonstration of a full-scale vehicle. This scheme could be used as a propulsion test vehicle.

Gyros can be used for angles and rates. Position could be measured as on the catapult or using a linear displacement transducer with an on-board battery. A tape recorder could store this data if the model is large enough. However, the same fundamental question of how to obtain the stability derivatives from position measurement remains.

3.2.3. Wind tunnel techniques

(1) Fixed images

For this scheme to be useful, all boundary layers must be thin compared with characteristic lengths, such as the lateral clearance δ and the vertical clearance h. Some investigation is needed to show that the coupling between the boundary layer and pressure distribution is the same with a solid guideway as with images when the boundary becomes thick. This scheme uses standard instrumentation and data handling.

At least six models would be required to simulate both the ground plane and the side walls. The wind tunnel cross section would look as follows:

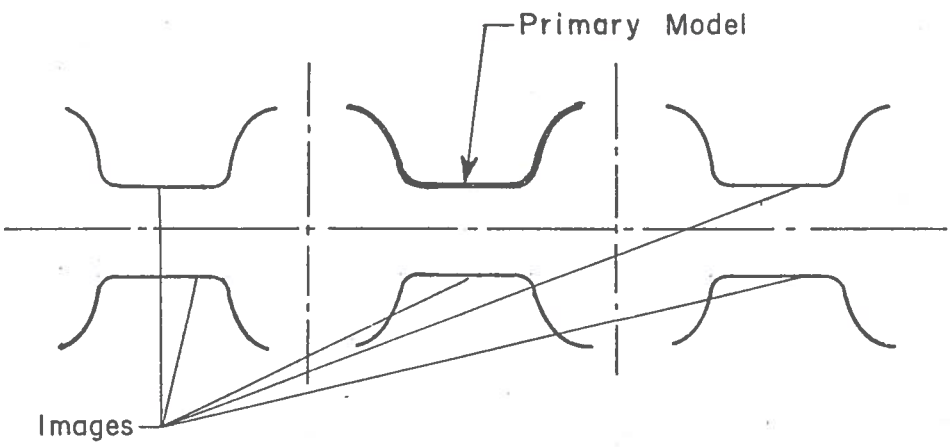

CROSS SECTION OF THE WIND TUNNEL

(2) moving belt

This scheme is a conventional scheme of wind tunnel testing with a moving guideway. If the guideway has straight sides, then very little new technology is involved. Speeds here are limited to 100 - 150 mph because of limitations in moving wall velocities. Corner joints may cause difficulties.

(3) possible combinations

A somewhat detailed design of a moving belt can be found in references 7 and 10. As indicated above the instrumentation would be similar to any wind tunnel testing. The same comment applies to the image technique at least as far as the main model is concerned.

Apart from the solution of having six models to simulate both the ground and the side walls, the following simpler designs could be considered.

TWO IMAGE MODELS AND SIDE WALLS

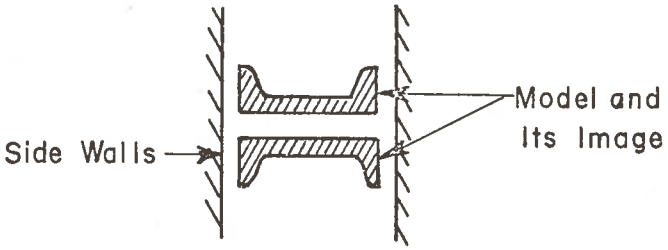

TWO IMAGE MODELS AND SIDE MOVING BELTS

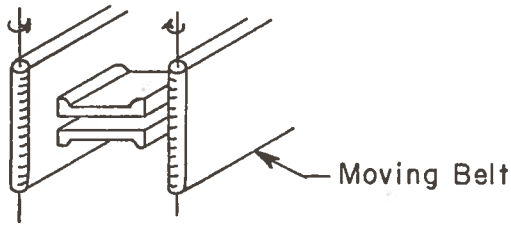

These designs would give the testing a lot more flexibility, the price being some unknown effects either due to the side walls or the moving belts. Of course the configuration is restricted to rectangular guideways.

However, it seems inadequate to adopt any of the wind tunnel solutions without further information about the ground or side wall effects. A separate study of what happens near the wall could be performed using the following configuration:

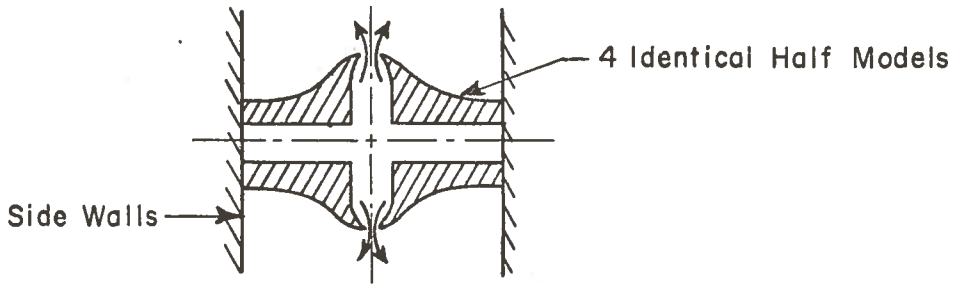

This together with a comparison of the results reported in ref. 11 with the same experiment using a simple board to simulate the ground, would perhaps allow one to obtain the necessary information about the boundary effects. The possibility of deducing some kind of correction for the incorrect boundary simulation would probably determine how suitable the wind tunnel is for testing ram wing vehicles.

TABLE II

Symbols

blank: the item is provided.

\- : the item is not necessary.

X : the item is a source of difficulty or uncertainty.

* : it is impossible to provide the item.

		Belt	Image	Catapult	Self propelled	Whirling arm	Towing tank (H_2O)	Towing test (air)
Fundamental	True simulation	X	X			X		
	No boundary layer problem	X	X			X		
	No "unknown effects"	X	X			X	X	X
Instrum.	Forces and moments easy to measure			*	*	X	X	
	Trajectory known accurately	-	-	X	X			
	Easy to measure quantities continuously			X	X			
	Derivatives of position W.R.T. time not necessary			X	X			
	Gyros can be used for angles & rates	-	-	*		-	-	-
	The test is not too short			X	X			
Flexibility	Easy to make model changes		X		X			
	Possible for all track config.	*	*		X			
	Control of trajectory	-	-	*				
	Forced motions possible		*	*				
	Dynamic testing possible		*	X	X	X	X	
	Flight visualization possible	*	*			*	*	
	Can be used for quick estimations	*	*		*	*	*	X
Tech Prob	Easy to position and align	X	X				X	X
	No waterproofing problem						X	
Other	Known technique						X	
	Not expensive model				X			
	Not expensive set-up	X	X		X	X	X	X
	No time constraint	X				X	X	X
	Not much space required				X	X		X

3.3. Advantages and Disadvantages

Table II compares the seven methods in terms of desirable characteristics. These characteristics are grouped in five main categories:

- Fundamentals: discussion of the value of the principles underlying the method.
- Instrumentation and data: what can be measured and how easily.
- Flexibility
- Technical problems
- Others

These categories and some of the less obvious reasons for the classification are discussed below.

3.3.1. True simulation

The powered model or glide test is indeed the best simulation of the full-scale phenomenon as the model is actually flying. The next best simulation is probably the air or water towing tank. All the other solutions are somewhat arbitrary in the way either the ground (belt-image), the model (whirling arm) or the atmosphere (wake effects in the whirling arm) is simulated.

3.3.2. Boundary layer effects

Let us compute the Reynolds number Re

Wind tunnel glide test: $c = 4$ ft $U = 40$ ft/s $Re = 10^6$

Towing tank: $c = 4$ ft. $U = 2$ ft/s $Re = 0.7 \times 10^6$

Full-scale model: $c = 100$ ft. $U = 300$ mph $Re = 270 \times 10^6$

As discussed in the preceding paragraph, there is a general problem as far as Reynolds number is concerned. Transition might be a problem especially considering the very small clearances from the ground or the side walls that we are interested in. However, this problem is common to all the techniques and hopefully will not be too significant.

3.3.3. "Unknown" effects

This term is meant to denote effects linked to the principle of the system itself that can be recognized in advance.

The whirling arm technique suffers from several phenomena. The curvature and centrifugal effects would probably influence the measurement of the moments. Some corrections would have to be defined, but this effect being of the "potential flow" type, it might even be possible to compute it theoretically. Because the gap is very small, the induced flow in the sides of the model would probably be negligible. Because of the length of the model, on the contrary, the centrifugal forces might indeed cause a deviation of the streamlines. This effect can only be estimated by a detailed calculation or the experiment itself.

An even greater problem with this technique is that the model is constantly flying in its own wake. This "viscous" type effect could be very serious as no correction could be computed easily. The uncertainty it creates is an argument against this method.

The moving belt technique also suffers an unknown effect due to belt waviness. In reference 3 a waviness of the order of 0.02 inch is reported. This is not negligible compared to our clearances. Even assuming that this could be reduced to a smaller amount the effect of a nonplanar ground might not be negligible.

3.3.4. Computation problems

The catapult or self-propulsion methods prohibit all measurement of forces or moments. Therefore the stability derivatives should be obtained from position measurements. As can readily be expected, the continuous measurement of six quantities (three angles, two displacements, and one velocity) with the kind of accuracy that is required in a stability analysis, proves to be a very tough problem (especially since the derivatives of data with respect to time are required). Though this can be done in theory, it would probably create serious computation problems and the precision would be uncertain, as results and experience with firing range and ballistic tunnels would show.

3.3.5. Dynamic testing - forced motion

The derivation of Appendix A shows that eight dynamic derivatives have to be determined; it would be good if some of them could be obtained experimentally. In a wind tunnel, in the towing tank or whirling arm it is in principle possible to vary any parameter continuously, despite some technical difficulties. This has indeed been done (ref 17) in the study

of submarines. However, it would be very difficult to use the image technique for this purpose as one would have two to six models in phase with a very high degree of accuracy.

3.3.6. Track configuration

At this stage of the design of ram wing vehicles no optimization of the shape of the cross section of the track or the model has been achieved and this is one of the results expected from this experiment. Therefore flexibility in changing the shape is desirable.

The moving guideway would probably have to be restricted to flat bottoms and sides (vertical or inclined) and the "image" to flat bottom and vertical sides. Unless it can be shown by another method that a rectangular track must be chosen this limitation is a strong argument against these techniques.

It is to be added that a self-propelled model requires a long and accurate track. Any modification would be very costly although possible.

3,3.7. Positioning

In the glide test the track needs only be aligned once, and this is very easy.

With a moving belt one model has to be positioned using usual wind tunnel techniques.

If the image technique is used the main model can be positioned as usual, but one to five models have to be adjusted with respect to the main model with high accuracy. This could prove to be a source of difficulty.

3.3.8. Alignment

In either type of towing test (air or water) the alignment of the track and the carriage would have to be very precise (probably of the order of one mil). This would only have to be done once. The position of the model in the track would have to be known during the motion and this will be discussed later.

If a whirling arm is used and the guideway is assumed to be a perfect circle, the only problem would be to position the axis of the arm right at the center of the circle. This should not be difficult (and in any case a variation from the ideal could easily be measured, and perhaps used to advantage).

3.3.9. Waterproofing

This obviously only applied to the tests conducted in water. The solution of waterproofing the model itself is not acceptable. (The waterproofing would have to be done without applying any force to the supporting arm which also bears the strain gage balances.) Each device such as transducers, strain gages, etc. would have to be waterproofed separately.

3.3.10 Vibrations

This problem might be important in all the moving carriage techniques. However, this should more easily be solved in a water tank because of the very slow speed being used.

3.4. Conclusions

From the above analysis we can draw the following simple and partial conclusions concerning the choice of a method to test ram wing vehicles:

- The main problem with the moving belt would be to develop the belt technique itself. Its drawback seems to be the imperfect simulation and that track configurations are limited.
- The difficulty with the image technique would probably arise from its lack of flexibility: limited configurations, difficult dynamic testing, difficult positioning and changes.
- The catapult seems attractive because of its flexibility and the simple set-up. The main difficulty to solve would be the instrumentation.
- The self-propelled model is obviously the nearest to a full-scale prototype. Instrumentation and general design would be difficult and expensive.
- The towed model would raise some problems of technology and instrumentation; however, no major inconvenience has been found, and the simulation is good. For reasons of greater availability of facilities the use of water seems to be the most practical.
- The whirling arm poses problems similar to the towing tank, but the simulation is not as good because of the curvature and the wake effects. Moreover they are not available as are towing tanks.

The advantages of each of the possible methods have been discussed. Before one can be chosen in preference to the others, the purpose of the experiment in terms of short and long term goals should be defined more precisely. Side considerations such as money, time available, existing facilities etc. should be taken into account. The primary conclusion reached here is that there is no single facility or test technique that is clearly better than the other six discussed. In the long term a tracked system in air has much to offer, particularly if fitted with a non-interfering magnetic suspension system. In the short term it may be necessary to eke the data out from different facilities.

CHAPTER 4

THE TOWING TANK EXPERIMENT -- DESCRIPTION

4.1. General

Since glide tests have already demonstrated the validity of the concept itself, the greatest interest lies in reliable quantitative measurements. On the basis of the survey in Chapter 3 the towing tank technique was considered the cheapest and quickest way to obtain the stability derivatives of a ram wing vehicle.

Two series of tests are referred to in this report that took place at an interval of three months. The first experiment was ended before extensive data could be obtained by a structural failure of the balance. For this reason information was obtained only on lift, drag and pitching moment. These results, if incomplete, were good enough to justify a second run for which some improvements were made, that are described below together with the general description of the setup.

4.2. The Tank

The towing tank of the Naval Architecture Department of MIT, which is located in the Hydrodynamic Building was used for this experiment. The tank is 8 feet wide and 80 feet long. The water is about 4 feet deep which is considered enough at this stage to avoid any major interference of the surface. A general view is reported in Fig. 1.

4.3. The Carriage

The carriage can be seen on Figs. 1 and 3. The carriage is supported and guided by wheels along two cylindrical rails. The alignment of the rails can be completed with a high degree of accuracy, although it was easier for our purpose to align the guideway directly with respect to the carriage. When the carriage is heavily loaded the speed range is between 0.2 and 4 knots. At the selected speed of 3.36 ft/sec the velocity can be considered constant for 40 ft. out of the total 80 ft.

4.4. The Orientation System

The orientation system (cf Fig. 3) was designed to allow for adjustment of side position, ground clearance and angle of attack. Essentially it consists of three threaded shafts, two at the front to vary the height, and one at the back to vary angle of attack. The axis of rotation was located so that α could be varied between 0 and 2 degrees with a variation of ε_o (the ground elearance below the center of resolution) smaller than 0.006 inch which can be neglected. The variation reaches 0.046 inch at 3.5°; this could be either compensated for or neglected again since it appears that the stability derivatives do not depend as strongly on ε_o as they do on α. Tne true values of α and ε_o could be obtained from the position sensors.

The side displacement capability was improved between the first and second series of tests. The improvement consisted of two 1/2" diameter rods on the carriage along which five ball

bushings linked to the model can slide. Friction is very small and the model can be maintained in any position by simply using shaft collars. No yaw adjustment was explicitly provided. However, a very little differential action on the two front threaded shafts could vary the yaw angle as much as required without introducing any significant roll angle.

The adjustment of roll was provided at the model itself and is described in Par. 4.8.

4.5. The Guideway

The U-shaped guideway is 12 inches wide, 6 inches high and 72 feet long. For the first series of measurements the guideway had a bottom made out of 1/16 inch thick brass reinforced by cross brass angles, one side also made out of brass, 1/8 inch thick, and finally the second side was made out of plexiglass so that the model could be observed and eventually filmed. A general view of the guideway is reported in Fig. 1, and a cross-section schematic drawing is shown in Fig. 18.

Because the side clearance is very small and is critical, the guideway had to have a very constant width. It was first hoped that the sections could be built with a maximum width variation of $\pm$ 0.010 inch.

This proved difficult to achieve with the time and money that were available. Finally most of the sections were separately aligned within $\pm$ 0.025 inch on the width and $\pm$ 0.010 inch on the perpendicularity of the sides. The nine sections, each eight feet long, had to be aligned together and with respect

to the carriage at the bottom of the tank. This was done by using a dial gage attached to the carriage as shown in Fig. 1. After the final alignment it was estimated that most of the track had a width of 1 foot $\pm$ 0.030 inches with the exception of a few locations at + or - 0.050 inch. Since a relatively large side gap (δ_o = 1/4" or $\hat{\delta}_o$ = 0.04) was chosen for this first series of tests, this alignment could be considered satisfactory.

Since the performance of ram wing vehicles of the type considered are highly improved by having as small a side clearance as possible it was decided to adopt δ_o = 1/8" or $\hat{\delta}_o$ = 0.02 for the second series of measurements. When the model is displaced by 1/16" either to the left or to the right, the gap is reduced to 1/16". This requires an alignment of the guideway to an accuracy that could not be reached with the scheme used previously. It was therefore decided to modify two of the nine sections (16 feet) which would give a long enough steady state reading.

The new sections use the same brass sheet at the bottom, but the sides are now 6" wide aluminum channels (3/16" thick). Each side can be adjusted at three locations using a screw and nut combination to within $\pm$ 0.015 inch. The width of these sections is reduced to 11 3/4" while that of the remaining ones is unchanged. The aluminum was anodized to avoid corrosion.

4.6. The Position Sensors

Five non-contact induction position sensors were used to give the complete attitude of the model in the guideway (side

position, yaw angle, ground clearance, angle of attack and roll angle). If the guideway was perfectly aligned and the whole structure supporting the model rigid enough to give zero deflection under maximum load, these sensors would not be necessary, since the attitude could be measured when the model was at rest, before each run, using, for example, optical methods.

The sensors are located as indicated below in the sketch; the maximum range is indicated in parenthesis. The output is between 0 and 1 volt for the entire range and a resolution of 5 to 10 thousandths can be easily obtained.

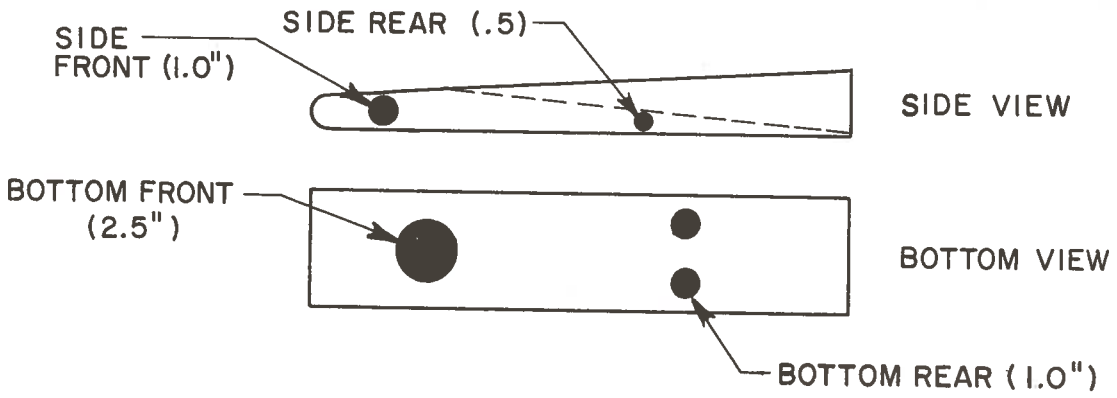

However, some difficulties were encountered during the first experiment. The three bottom sensors were calibrated, once mounted in the model, by elevating the whole model above the bottom of the guideway using spacers. The calibration curves were later recorded by elevating the model a known amount using the model orentation system. This yielded usable results although linearity was poor.

Since the two side sensors were only directly surrounded by epoxy and wood it had been assumed that their calibration could be performed on a calibration jig in water. This assumption turned out to be completely wrong yielding saturation of the two sensors at any location in the guideway. They were finally calibrated very roughly using the side displacement capability of the orientation system, but it was recognized that a new procedure would have to be generated for calibration.

The New Calibration Procedure

The orientation system was modified as described before to be used with ease to calibrate the two side sensors.

The three bottom sensors are calibrated using steps at the bottom as shown in the sketch below.

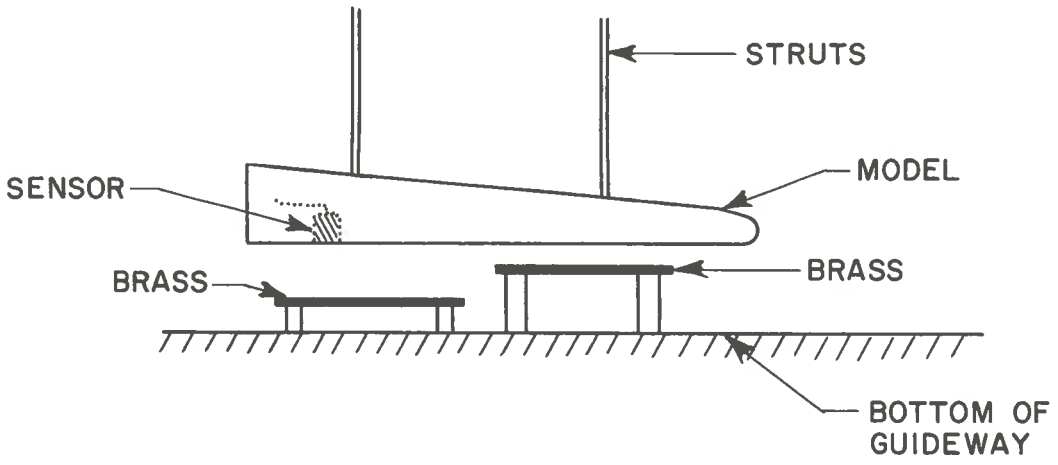

and by positioning the carriage alternately over the different steps, which have a known height and are made out of brass of the same thickness as the bottom of the guideway.

4.7. The Force Balance

A six-component force balance was designed by Teledyne Materials Research of Waltham, Mass. for this experiment. It is composed of two parts located at each of the two struts supporting the model. The forward portion measures "forward" lift, rolling moment, "forward" side force and drag. The aft portion measures aft lift and aft side force. The pitching and yawing moments can easily be obtained by linear combination.

The interaction matrix as obtained from the balance calibration is as follows:

$$\begin{bmatrix} \overline{L}_o/100 \\ AL_o/50 \\ S_o/10 \\ AS_o/10 \\ R_o/100 \\ D_o/20 \end{bmatrix} = \begin{bmatrix} 1 & 0.0239 & 0 & 0 & 0 & -0.132 \\ 0 & 1 & 0 & 0 & 0 & 0 \\ 0.0588 & 0 & 1 & -0.153 & -0.0377 & 0 \\ 0 & 0 & -0.134 & 1 & 0.0485 & 0.0217 \\ -0.168 & 0 & 0.024 & 0.0289 & 1 & 0 \\ 0.0146 & 0 & 0 & 0 & 0.0591 & 1 \end{bmatrix} \begin{bmatrix} \overline{L}/L_m \\ AL/AL_m \\ S/S_m \\ AS/AS_m \\ R/R_m \\ D/D_m \end{bmatrix}$$

where L_o, AL_o, S_o, AS_o and D_o are respectively the lift, aft lift, side force, aft side force and drag expressed in lb. and R_o the roll in lb-inch. L, AL, S, AS, R and D are the readings from the actual processing devices that are being used, L_m, AL_m, S_m, AS_m, R_m and D_m being the corresponding values for maximum load.

According to the designer, the interaction matrix is repeatable to better than 3 percent. Although a complete recalibration could not be performed under water because of time limitation it was checked that under maximum load the main outputs were unchanged. On Fig. 1 the balance is shown on its calibration frame during "dry" calibration before the test.

The failure that ended the first test was repaired by the initial designer and a "stop" was built in the rear part of the balance that limits its up and down motion to 0.005 inch.

4.8. The Model

A schematic drawing of the model is shown in Fig. 19.

The model that was used during the first series of tests had balsa wood removable sides, covered with epoxy and paint for waterproofing. In addition to potential warping problems the thickness of these sides varied by as much as 1/8 inch along the chord. They were replaced by fiberglass sides of identical shape but closer tolerance. The width of the model can be considered constant within $\pm$ 0.020 inch. Most of the rest of the body is made out of anodized aluminum. The covering plate and the strut shields are not adequate to "smooth" the model, but since drag measurements are not the prime interest of this experiment this was considered to be acceptable.

The model is attached under the balance by means of four screws and two transversal aluminum pieces. By machining these two pieces at an angle, the model may be given a roll angle with respect to the balance and thus with respect to the guideway. Therefore to change the roll angle, it is necessary to remove

the covering plates, separate the model from the balance, change the adjusting pieces and put everything together again. This operation can be somewhat time consuming since it must be performed under water. However, the roll angle was expected to be changed only a few times in the whole experiment. Provisions have been made to adjust roll at zero, 1.5 and 3 degrees. Fig. 2a shows the model supported by the two V struts and the two side sensors on the left side. Fig. 2b shows the model from the top without the covering plate. Finally the model can be seen in its guideway under water in Fig. 3.

4.9. Vibrations

Probably because of a poor initial design of the towing tank, the carriage is subject to important vibrations. These vibrations are only a minor inconvenience when ship model testing is concerned. However, we thought that some investigations were justified for our experiment. The vibration is essentially a back and forth motion with two dominant frequencies. A 20-cycle vibration was recognized as a natural frequency of the carriage (unloaded). Although this could probably be remedied easily this frequency was considered high enough not to interfere with our low frequency measurements.

A four to five cycle frequency vibration was also present with a more important amplitude. Several outside companies declared that the problem could not be solved because the frequency was too low.

After some investigations of our own we attributed the carriage vibration to a spring-mass type oscillator, with the carriage as the mass and the metallic driving tape as the spring. Some very simple calculations led to the construction of a spring damper unit which was mounted between the tape and the carriage. Little improvement resulted and the noise required filtering.

CHAPTER 5

DISCUSSION OF THE RESULTS

5.1 General Comments on the Experiment

All the expected data points were recorded as planned during the experiment. Unfortunately as it will be seen in the next section the quality of the measurements suffered from two major problems. First of all the force readings were degraded by defective amplifiers in the signal processing unit. It resulted in a "mixing" of the roll and lift channels by which both became linearly dependent on both roll and forward lift as evidenced by a recalibration after the test. Fortunately the response was repeatable so that some sense could be made out of the data. However, accuracy considerations prevented one from being able to invert the calibration data in order to extract both lift and roll from the lift and roll channels. It was first assumed that the rolling moment is negligible when the model has a symmetric attitude. (This assumption is certainly acceptable since the rolling moment stiffness was very small.) The lift signal can then be interpreted as depending only on lift. In the case of dissymetric attitudes it was assumed that the lift was identical to the corresponding symmetric attitude. Both the lift and roll signals can therefore lead to a value of the rolling moment. The fact that the two values obtained this way are of the same order

of magnitude gives us some confidence at least in the qualitative information obtained this way. The assumption of constant lift can be seriously questioned, however, since the aft lift, for example, varies slightly in both cases.

The second major problem was that of electronic noise. The data from the strain gage balance were recorded on a six-channel 1/2-inch tape recorder. Data reduction later revealed that the recorder had an increasingly irregular speed from the beginning to the end of the reel. This resulted, on half of the data, in both some additional, high frequency noise (which was not a problem) and in very bothering low frequency (.2Hz) shifts. The noise was identical on all of the six channels. Because of the low signal levels of side forces, some data were lost.

5.1.1. Behavior of the position sensors

Little information was obtained from the position sensors. They were intended to correlate the force readings with the model attitude in case of guideway misalignments or deflection of the supporting struts under the applied loads. Although the inductance sensors that were used had seemed to be both flexible and reliable during evaluative testing, their use in the environment of our experiment probed to be difficult. The new calibration procedure for the bottom sensors proved quite adequate. However, these three sensors finally had little use since very little

vertical deflection results from the increased pressure on the bottom of the model and small variations in the guideway height have little influence. The information from the side sensors, however, would be very useful since a significant lateral deflection may occur when the model is in a dissymmetric attitude. Before these can be used, two problems remain to be solved. Although the new calibration procedure yielded somewhat better results than the first test, it is still not adequate to monitor the small variations of side gap. Also, the side sensors were sensitive not only to their distance to the side wall but also to their position in the guideway and in particular to the height of the model. These considerations plus the above uncertainties meant that no meaningful correlation between the lateral forces and position could be obtained.

5.1.2. Behavior of the strain gage force balance

The balance itself behaved satisfactorily through the two series of tests. However, another accuracy problem should be mentioned here. The balance was designed so that the repeatability would be between 2 and 3% of the maximum load on each channel. This means that the uncertainties are about 2 lb, 1 lb, .2 lb, .2 lb, and .4 lb on lift, aft lift, side force, aft side force and drag respectively and 2 inch-pounds on the rolling moment. Because we are using only a small portion of the total range of the balance, these numbers get to be large compared to

the forces we want to measure. The lift, which can be as high as 30 lb, is certainly acceptable although there is some question about it at low angles of attack. However, the uncertainties are in a typical case 20% on total side force, 30% on yaw, 30% on drag, 80% on pitching moment (it should be noted that although this seems very high it corresponds to an error of only 1 inch in the location of the center of pressure along the chord, or 2.5% of the chord) and 50% on rolling moment. As the discussion of the results shows, the ability of measuring accurately the side position of the model is an absolute necessity if reliable lateral information is to be obtained from this test. The way the sensors are used should therefore be improved or a different type of sensor should be tried.

5.1.3. Data reduction

As expected, because of the carriage vibrations, the signal to noise ratio can be as low as one tenth. This makes any direct measurement very difficult apart from when the forces are very large. However, since all the data were recorded on magnetic tape it was possible to run the signals through a first order filter before they were recorded on chart paper. This method yields excellent results so that errors caused by the process of going through a tape recorder, a filter and a chart recorder are estimated at less than 5 percent. Figs. 4a and 4b respectively show a typical output from the main lift and the aft lift channels. Fig. 4c is the lift after the filter (reduced time scale) and amplification.

5.2. The Experimental Results

5.2.1. General

The results from two series of tests are reported here. Many modifications were made between the two runs to try and improve the testing technique. However, the only changes that affect the results are those concerning the model configuration. The main difference is that the side gap δ_o was decreased from 0.25 inch to 0.16 inch ($\hat{\delta}_o$ of 0.027 instead of 0.04) as allowed by the better alignment of the guideway. Another important change was the replacement of the trailing edge since it was noticed during the first run that the trailing edge was not aligned with the rest of the bottom surface but was angulated upward (about 2°). This fault yields a lower lift and increased nose-up moment. The results from the first series of tests were therefore compared to a computed estimate which includes this trailing edge effect. Finally it should be noted that new sides were made for the model which were straighter than the original sides and the model top fairings were modified.

5.2.2. Description of the data

Only the angle of attack α and the height below the center of resolution ε_o were changed during the first experiment. Therefore only lift, pitching moment and drag are reported as a function of these parameters.

During the second test, in addition to varying α and ε_o, the model was also given nonsymmetric attitudes; namely, side

displacements of + and then - 1/16 inch and roll angles of -1.5° and -3°. (The model was rolled about the lip plane so that both the left and right side gap remained approximately equal to the nominal δ_o = 1/8 inch.) This would normally allow one to obtain four of the lateral derivatives. Because of troubles mentioned previously, three of these could not be obtained with satisfactory accuracy, and only the roll moment due to roll is reported here.

5.2.3. Lift

The variations of the lift coefficient with angle of attack for various clearances ε_o (below the center of resolution and not at the trailing edge) and two side gaps δ_o are reported in Figs. 5 to 7. The computed values almost always fall within 10 percent of the experimental data which can be considered very satisfactory since 10 percent is also the minimum uncertainty on the measurements.

On Figs. 8 and 9 C_L has been plotted versus ε_o for various angles of attack. The matching is good for $\hat{\delta}_o$ = 0.04 except at high values of ε_o. This discrepancy was expected since at these high values the lips of our model were higher than the sides of the guideway, thus increasing the side clearance considerably. For $\hat{\delta}_o$ = 0.027, however, we estimate a larger increase of lift with ε_o than experimentally obtained. As indicated in Chapter 2 many changes could be made to the mathematical model. However, improvements are not obvious because we overestimate lift at high ε_o and underestimate it at low ε_o.

C_L was plotted versus $\hat{\delta}_o$ for ε_o = 1 inch and three angles of attack on Fig. 10. This agrees fairly well with the experiment and some confidence is gained as to the way the side gap effects are calculated.

It should be emphasized that the matching of experimental and estimated lift is remakably good considering that neither trailing edge thickness nor leading edge effects were considered. This also shows that the thickness effect indeed contributed very little to the total lift.

5.2.4. Pitching moment

The variations of the pitch coefficient versus angle of attack for various clearances ε_o and two side gaps δ_o are reported in Figs. 11 to 13. The moments were computed with respect to half chord (X_o = 0.5).

At low angles of attack the results for $\hat{\delta}_o$ = 0.027 show a definite nose-down moment which does not exist at $\hat{\delta}_o$ = 0.04. This difference should probably be attributed to the difference in trailing edge angle that was mentioned previously. Our mathematical model could also predict this nose-down moment provided the assumption of free stream pressure at the trailing edge is removed. By assuming C_p = .2 at the trailing edge the computed estimate of C_M agrees satisfactorily with the experimental data up to $\alpha \sim 0.75°$. At higher angles of attack it seems that leading edge suction should be taken into account. Because the pitching moment seems to be fairly independent of

height as opposed to a large variation predicted by our mathematical model, it is possible that the thickness effect is responsible for some of the discrepancy even if its net effect on lift seems negligible. It should be noted that the difficulty of locating the center of the balance accurately with respect to a three-dimensional model does add some uncertainty. However, this cannot explain differences as large as 2 inches between the experimental and estimated locations of the center of pressure.

5.2.5. Drag

The lift-to-drag ratio L/D as a function of angle of attack is reported in Fig. 15 for $\hat{\delta}_o = 0.04$ and in Fig. 14 for $\hat{\delta}_o = 0.027$. The drag that was considered is the sum of the induced drag and of the body drag as measured by the force balance along the body axis. It turned out that for $\hat{\delta}_o = 0.04$ the body drag was essentially constant for all the attitudes considered and equal to 1.3 lb. This is in agreement with our theory which predicts that the momentum drag is approximately equal to the induced drag $L \cdot \alpha$. The body drag can then be interpreted as a pure constant viscous drag. However, the picture was slightly different for $\hat{\delta}_o = 0.027$. The body drag was not constant any more but decreased almost linearly from 1.8 lb to .6 lb at $\alpha = 2.5°$. This yields an appreciable increase in L/D, more than the increase in lift alone would predict. The values of L/D agree generally well with that obtained during the glide test experiment of Ref. 1.

5.2.6. The lateral derivatives

Because of the uncertainty in monitoring the side displacement, the variations of roll moment and side force with δ were not obtained with any degree of satisfaction and are not reported here. C_{ℓ_ϕ}, the nondimensional rolling moment due to roll angle, could only be obtained if it was assumed that the lift remained identical to the corresponding symmetric attitude, as already explained. The readings obtained this way from both the lift and roll channels are reported in Fig. 16. The scatter of the data gives some idea of the uncertainties involved. About the only conclusion that can be drawn from this plot is that C_{ℓ_ϕ} is negative for the larger angles of attack, so that the rolling moment is stabilizing. Also, when $\alpha = 2.5°$ (so that the lips of the model are essentially horizontal), the roll stiffness is of the same order of magnitude as predicted by the theory.

Chapter 6

CONCLUSIONS AND PERSPECTIVES

6.1. The Results

Because our efforts were concentrated on demonstrating the feasibility of this new testing technique, little new information was obtained on the ram wing vehicle dynamics in these two first series of tests. The basic idea that the side and trailing edge gaps are governing the flow was confirmed together with the fact that the thickness effect could in the first approximation be neglected with respect to the ground effect. The lift coefficients and L/D that were obtained are comparable with those from the glide test of ref 1.

6.2. The Testing Technique

The main purpose of this study was to set the theoretical and experimental bases for a preliminary design of a ram wing vehicle on the basis of its performance and its dynamic behavior. On viewing the experiment as a whole, we feel that the choice of the towing tank technique was justified for this purpose. However, we have not at this stage reached our initial goal of fully developing a reliable testing technique for future model configurations. Nevertheless we have acquired sufficient experience so that we feel that adequate instrumentation and procedures can be developed fairly easily in the near

future. The main problem that remains to be solved is that of accurate monitoring of the lateral position of the model in the guideway. It is also possible that the force balance will later have to be modified in order to reduce the range of forces and moments to be measured. With these improvements the testing should become more routine and the great advantage of this technique will then be that there is no limitation to the model shape and that the cost of any change to the model is limited.

6.3. The Mathematical Model

It is difficult to make a global judgment on the relevance of our mathematical model considering the limited experimental data available. The prediction of lift can certainly be considered very good considering the simplicity of our modeling. The main assumption that the side gap is the most important parameter in the description of the flow seems to be justified. The prediction of the variation of lift with the side gap or the angle of attack is very good too. Trailing edge and leading edge effects (important mainly at low and high angles of attack respectively) should certainly be included before the pitching moment can be predicted with some confidence. Until more data are available it is difficult to assess how accurately our mathematical model can predict the lateral derivatives. If the present experimental results are confirmed, some major changes would be required in the theory, other than the secondary improvements that have been mentioned in Chapter 2.

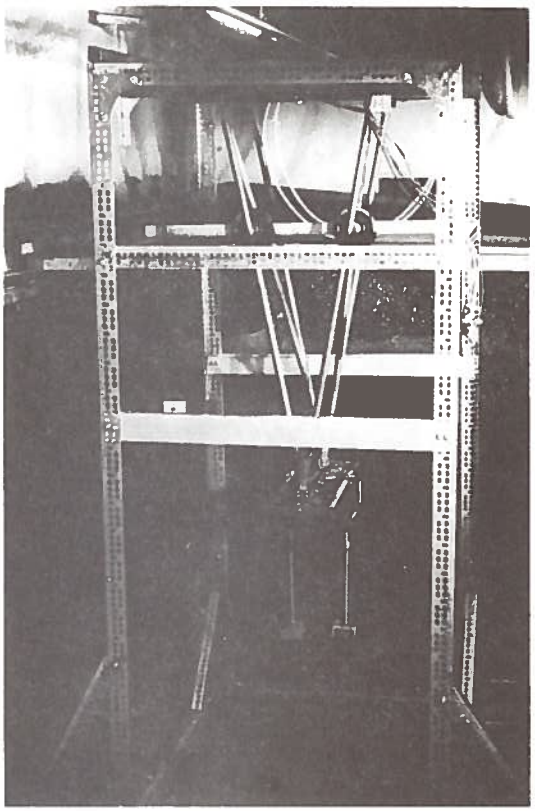

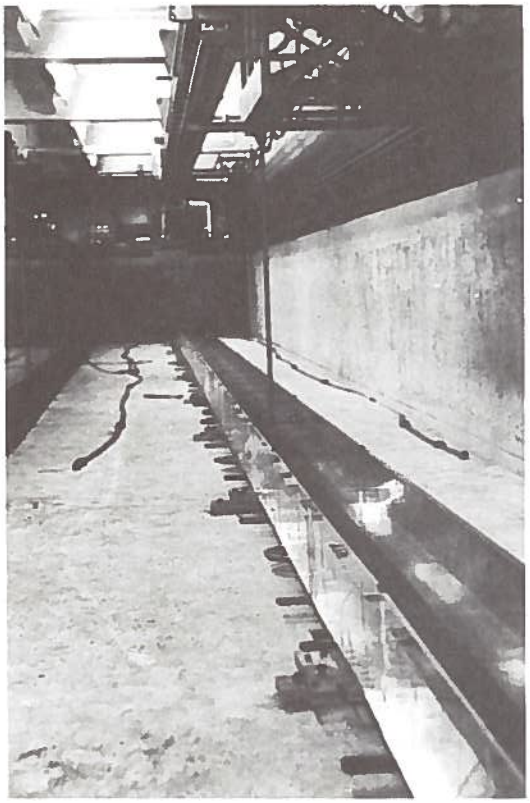

Fig. 1

Top: the balance on its calibration frame.

Bottom: general view of the tank, the carriage, and the guideway.

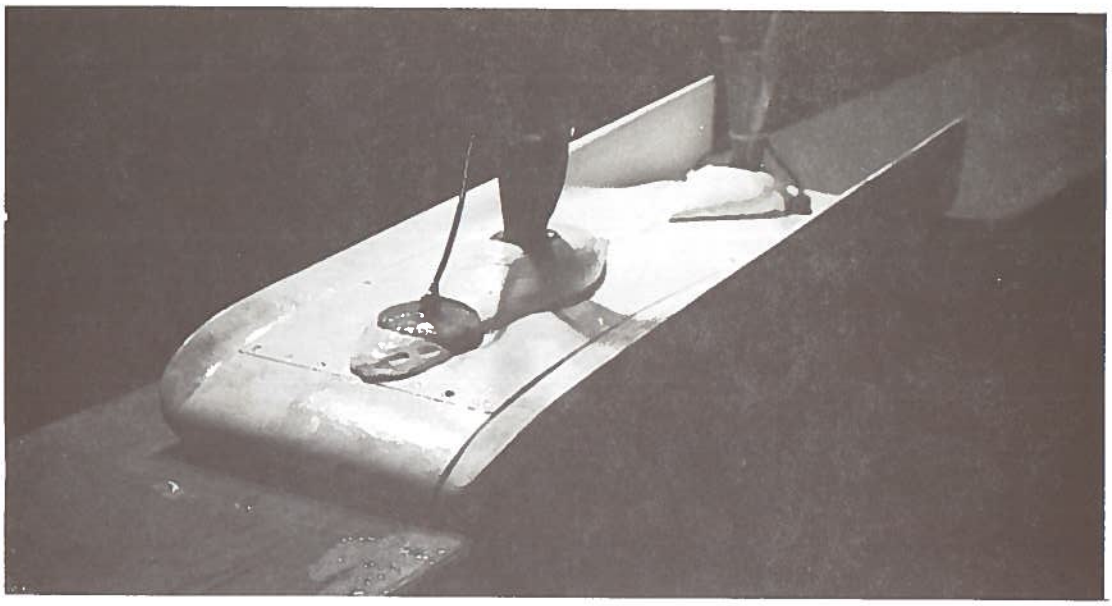

2a

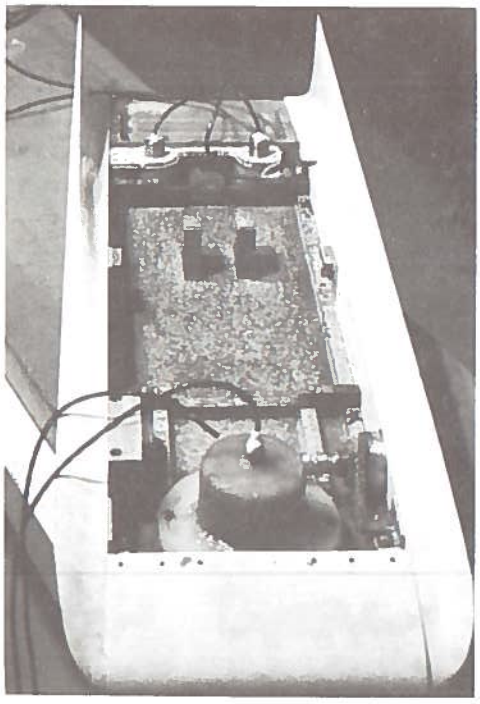

2b

Fig. 2. Two views of the model

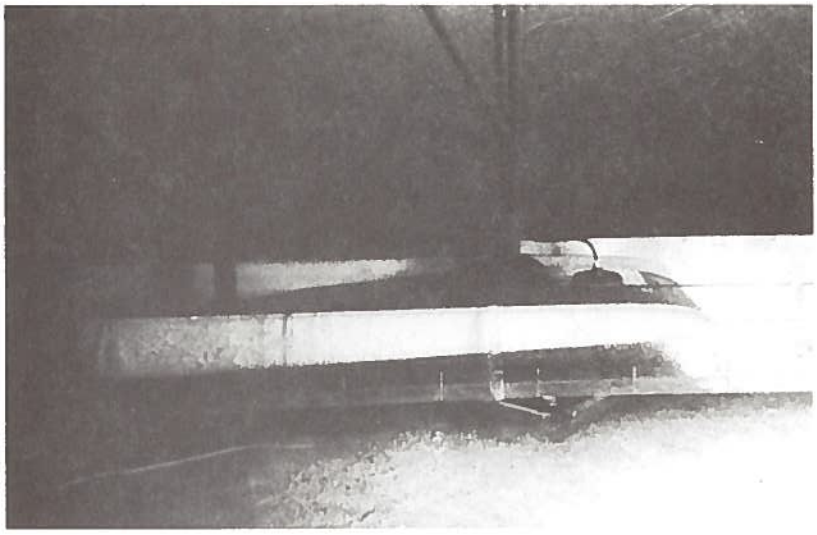

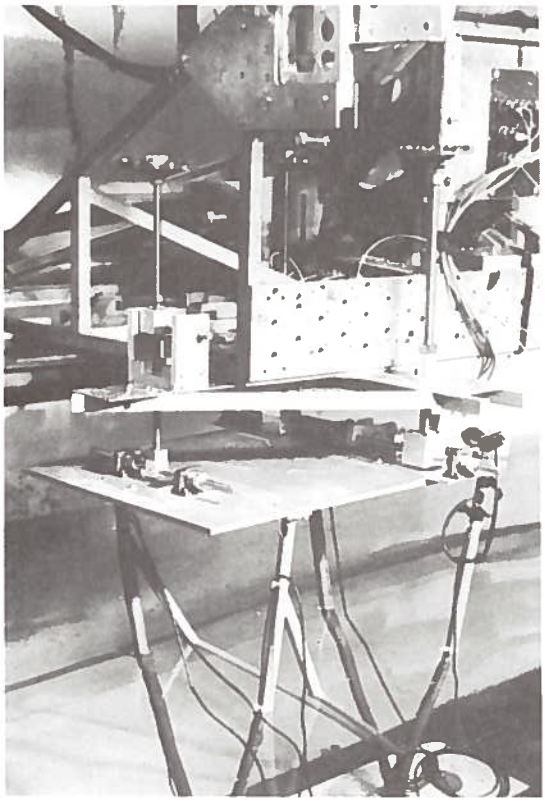

Fig. 3

Top: The first model in its guide-way under water

Bottom: The carriage and the orien-tation system

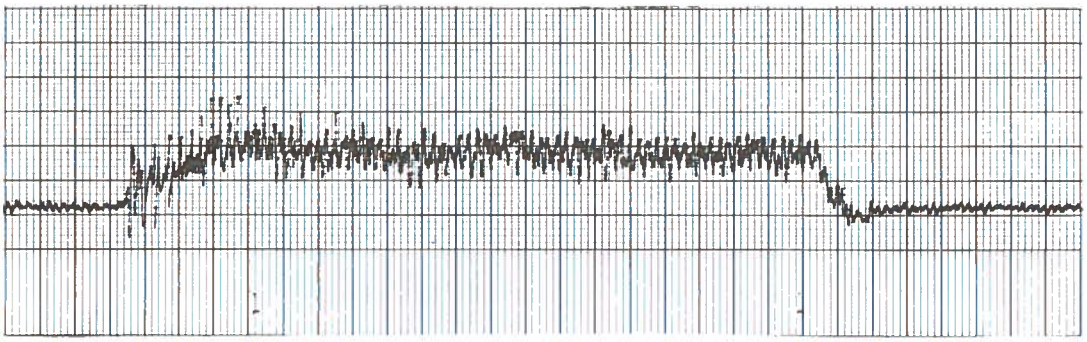

4a. Main lift

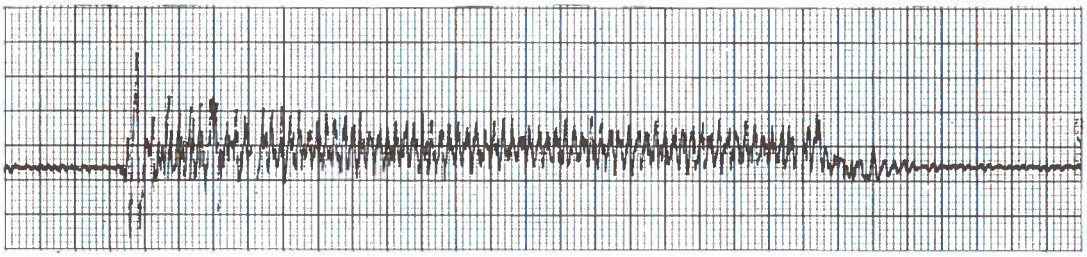

4b. Aft lift

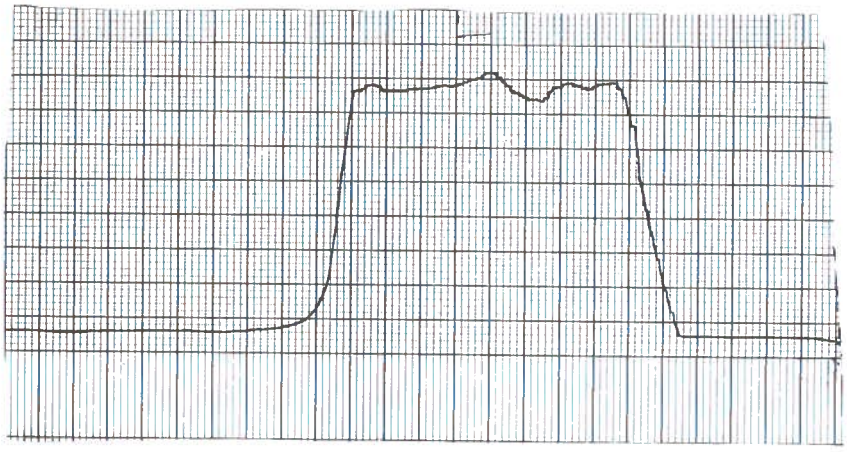

4c. Main lift after filtering

Fig. 4. Typical force output

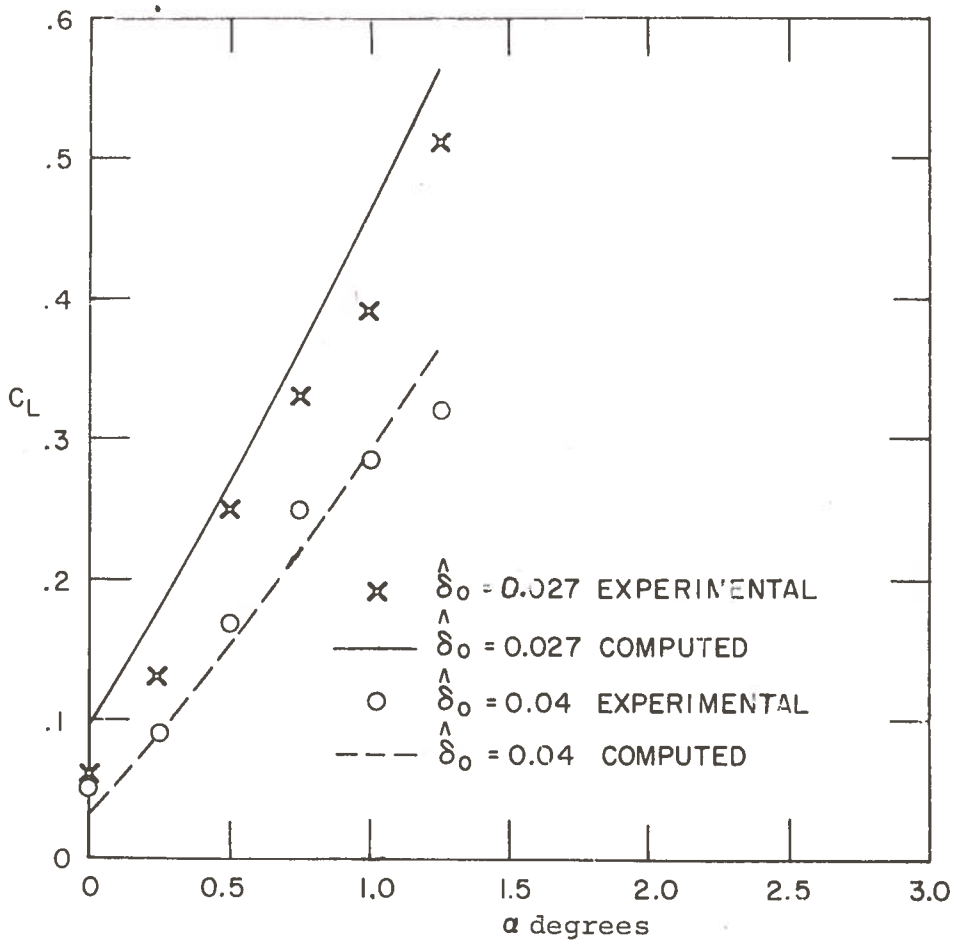

Fig. 5. Lift coefficient versus angle of attack for a clearance $\hat{\varepsilon}_0 = 0.0125$

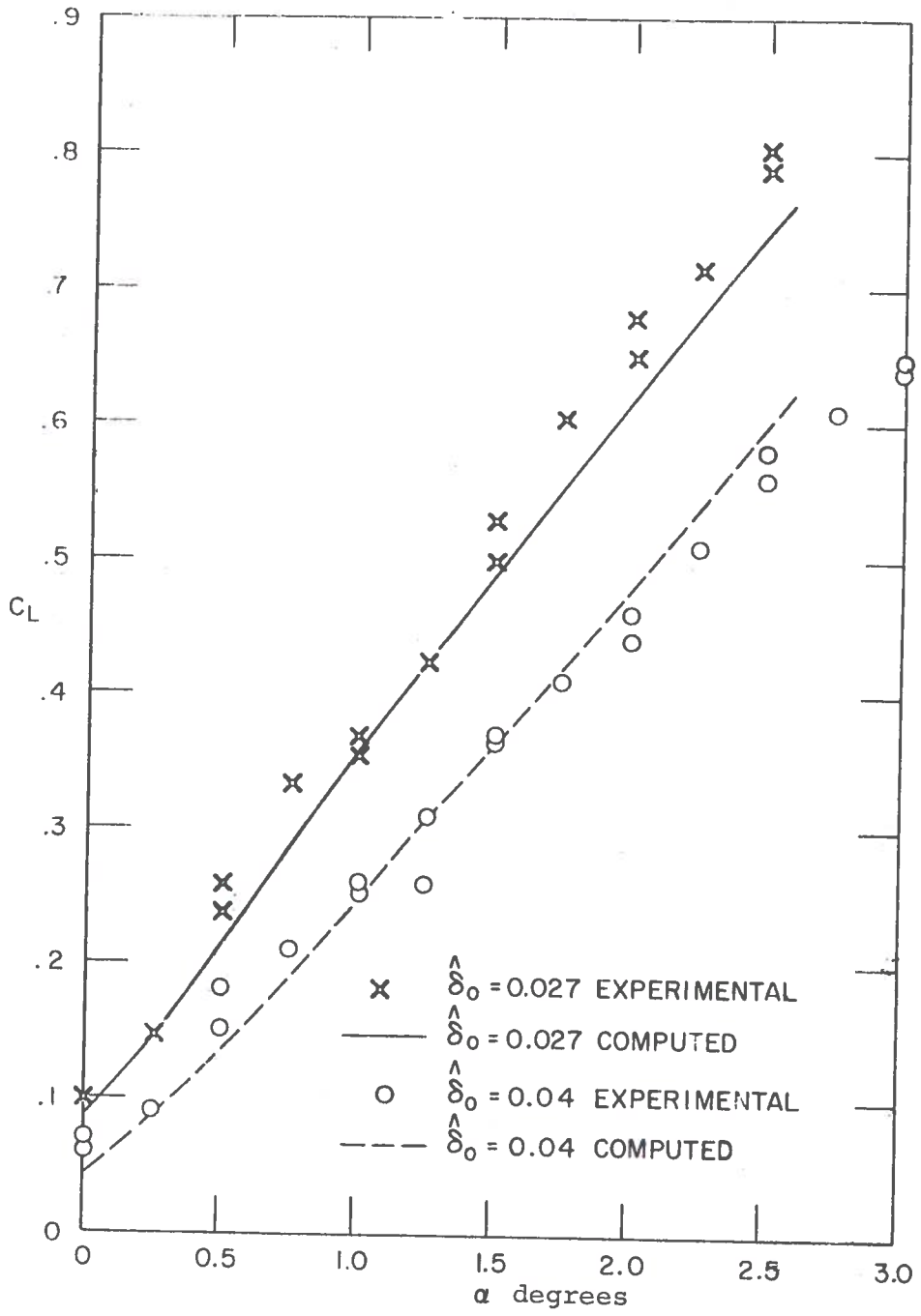

Fig. 6. Lift coefficient versus angle of attack for a ground clearance $\hat{\varepsilon}_0 = 0.025$

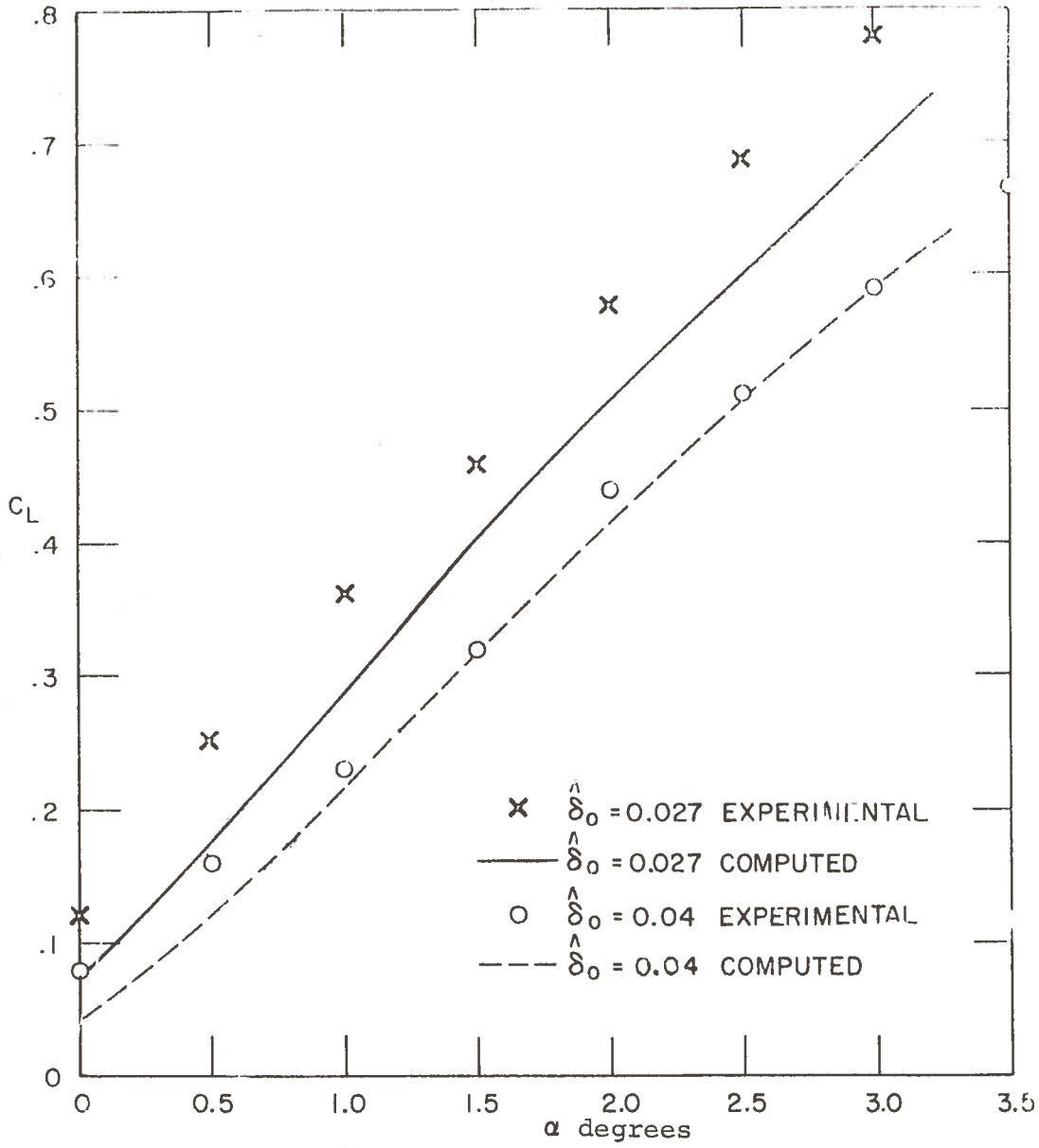

Fig. 7. Lift coefficient versus angle of attack for a clearance $\hat{\varepsilon}_0 = 0.0375$

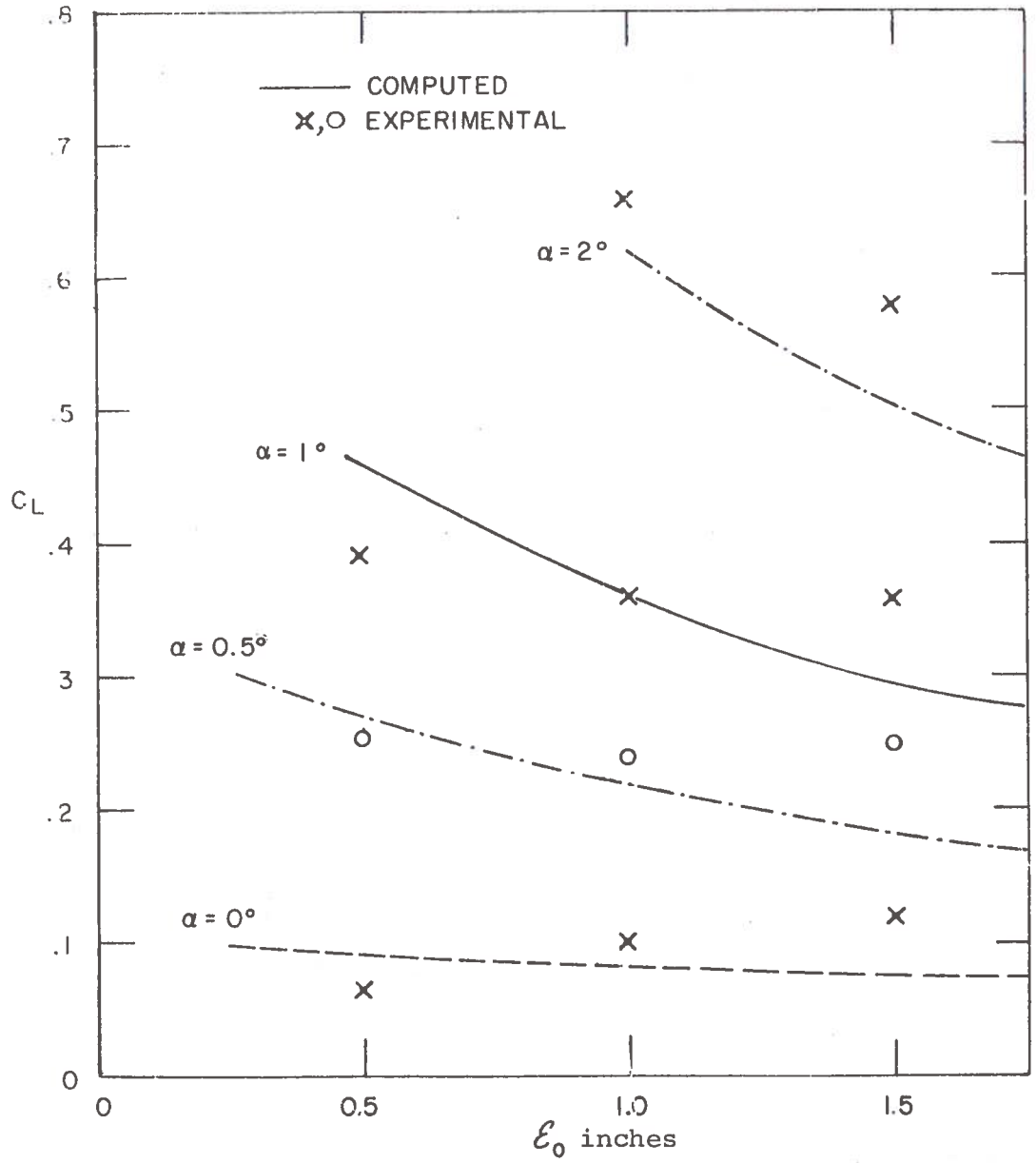

Fig. 8. Lift coefficient versus ground clearance ε_0 for various angles of attack and $\delta_0 = 0.027$

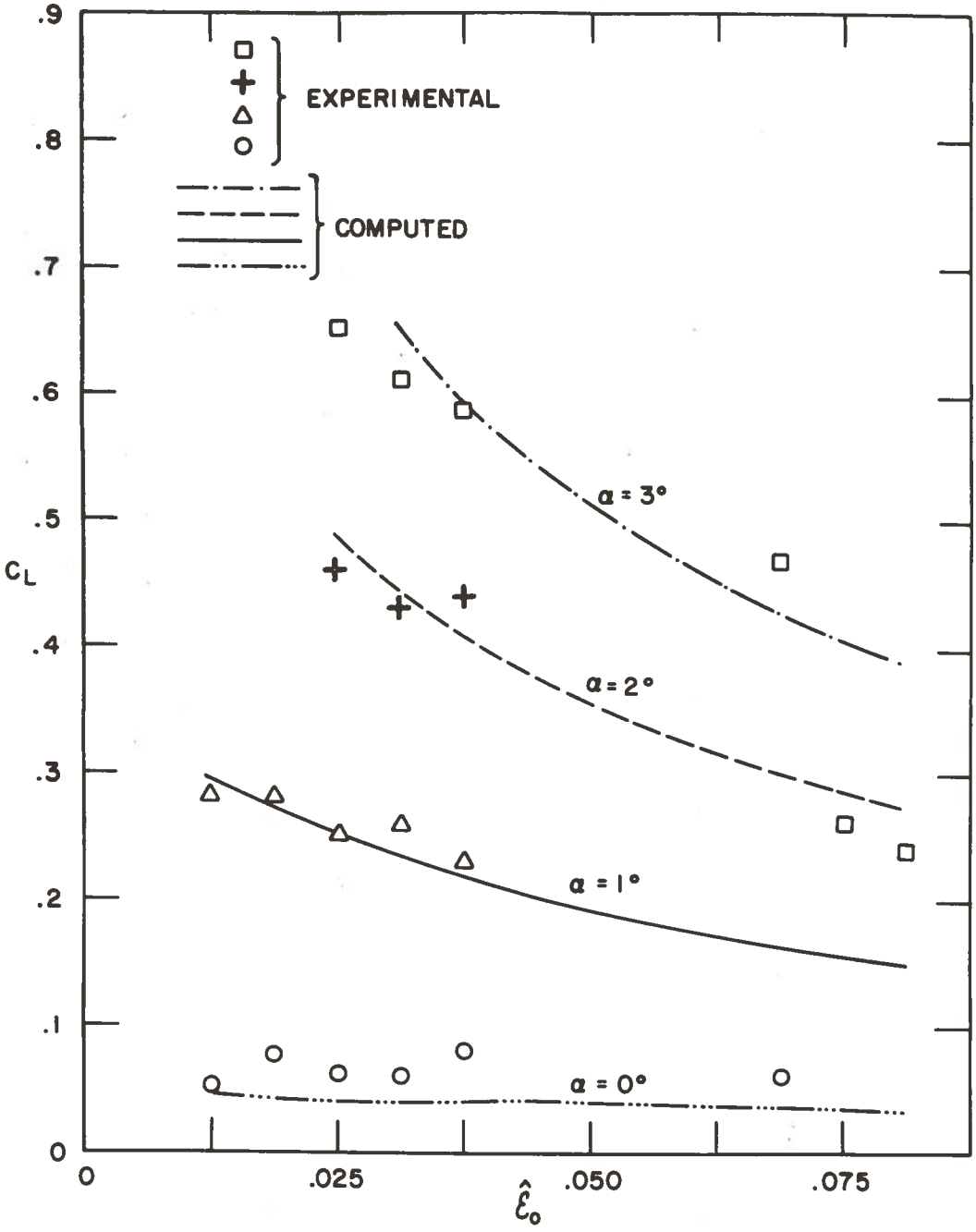

Fig. 9. Lift coefficient versus ground clearance $\hat{\varepsilon}_o$ for various angles of attack and $\hat{\delta}_o = 0.04$

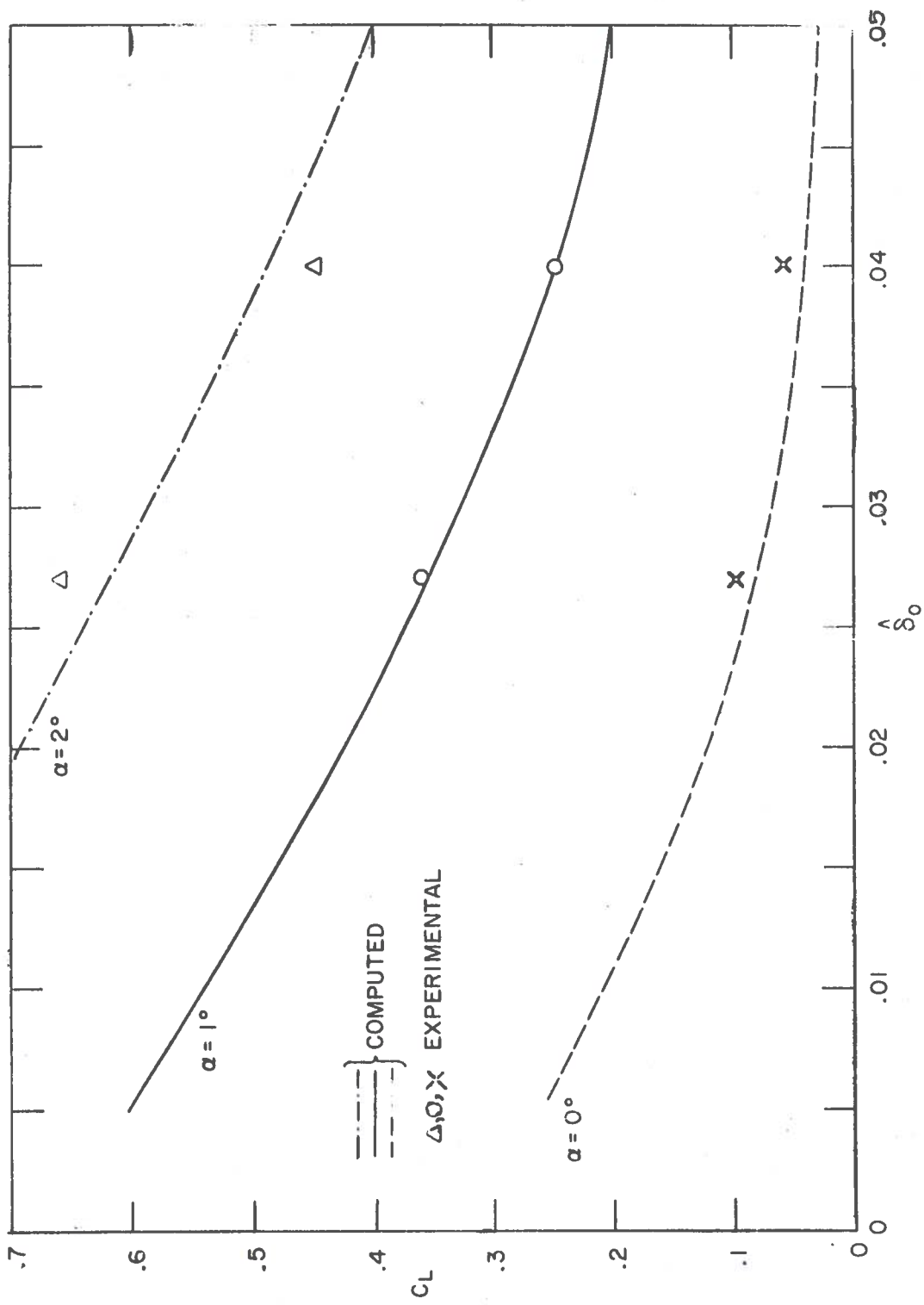

Fig. 10. Lift coefficient versus side gap for $\hat{\varepsilon}_o = 0.025$ and various angles of attack

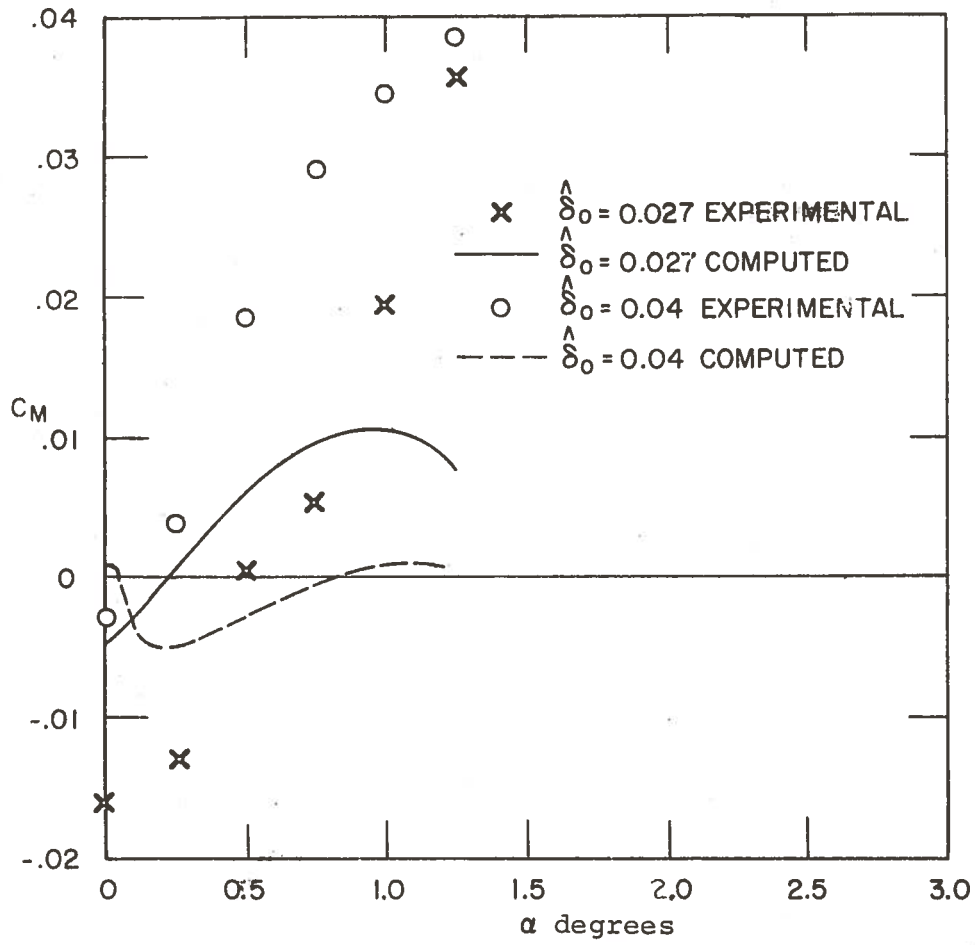

Fig. 11. Pitching moment versus angle of attack for $\hat{\varepsilon}_0 = 0.0125$

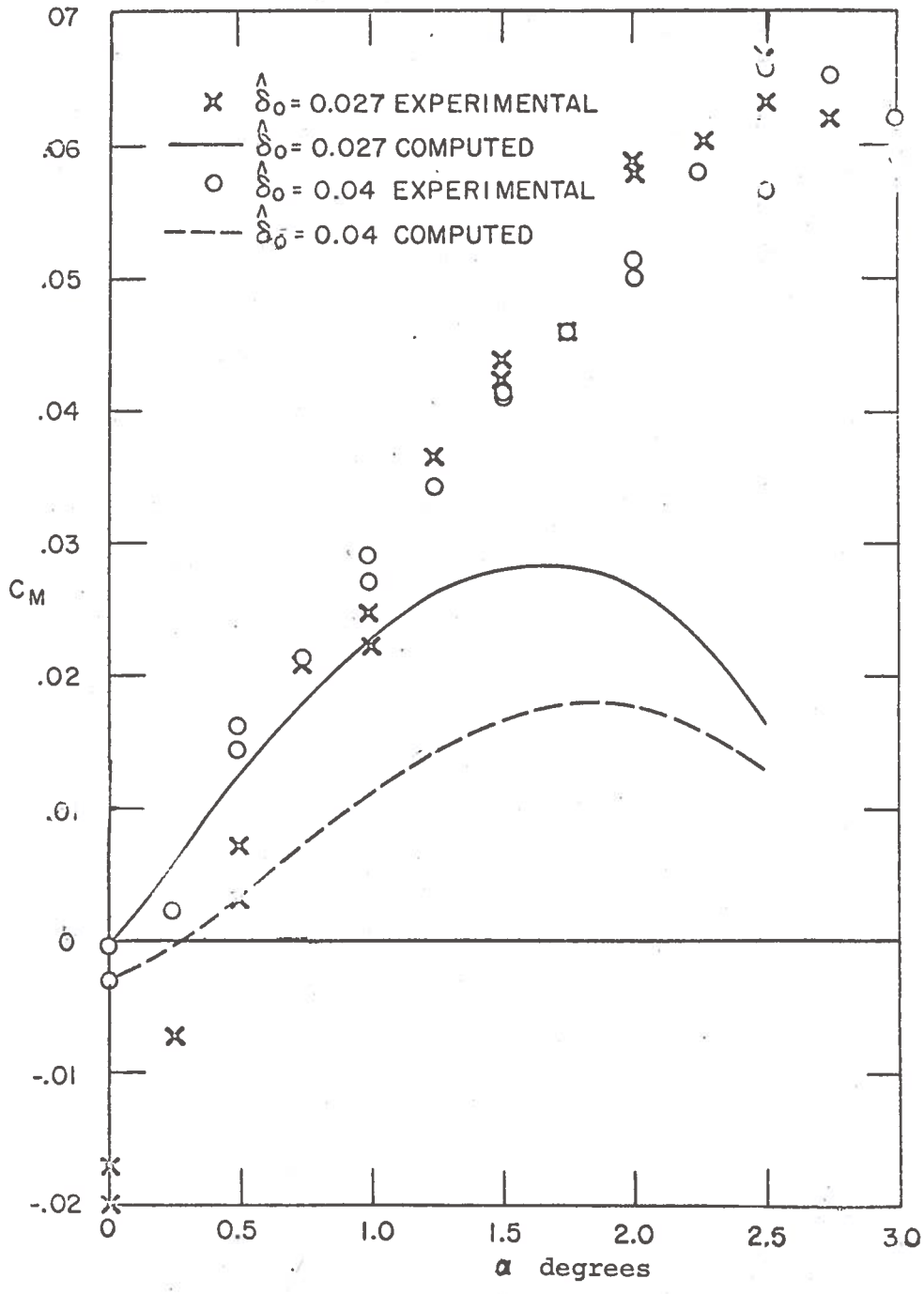

Fig. 12. Pitching moment versus angle of attack for $\hat{\epsilon}_o = 0.025$

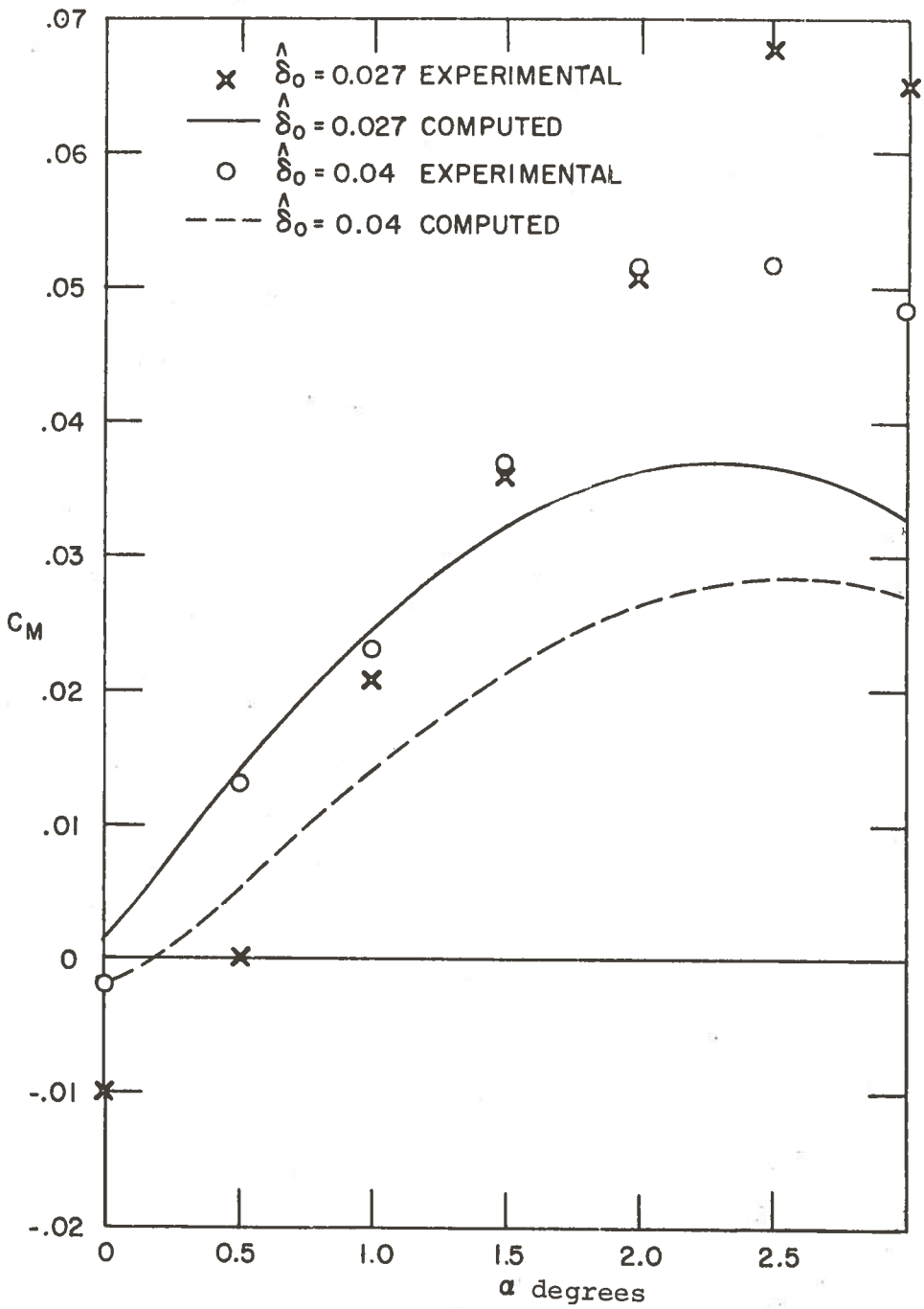

Fig. 13. Pitching moment versus angle of attack for $\hat{\varepsilon}_0 = 0.0375$

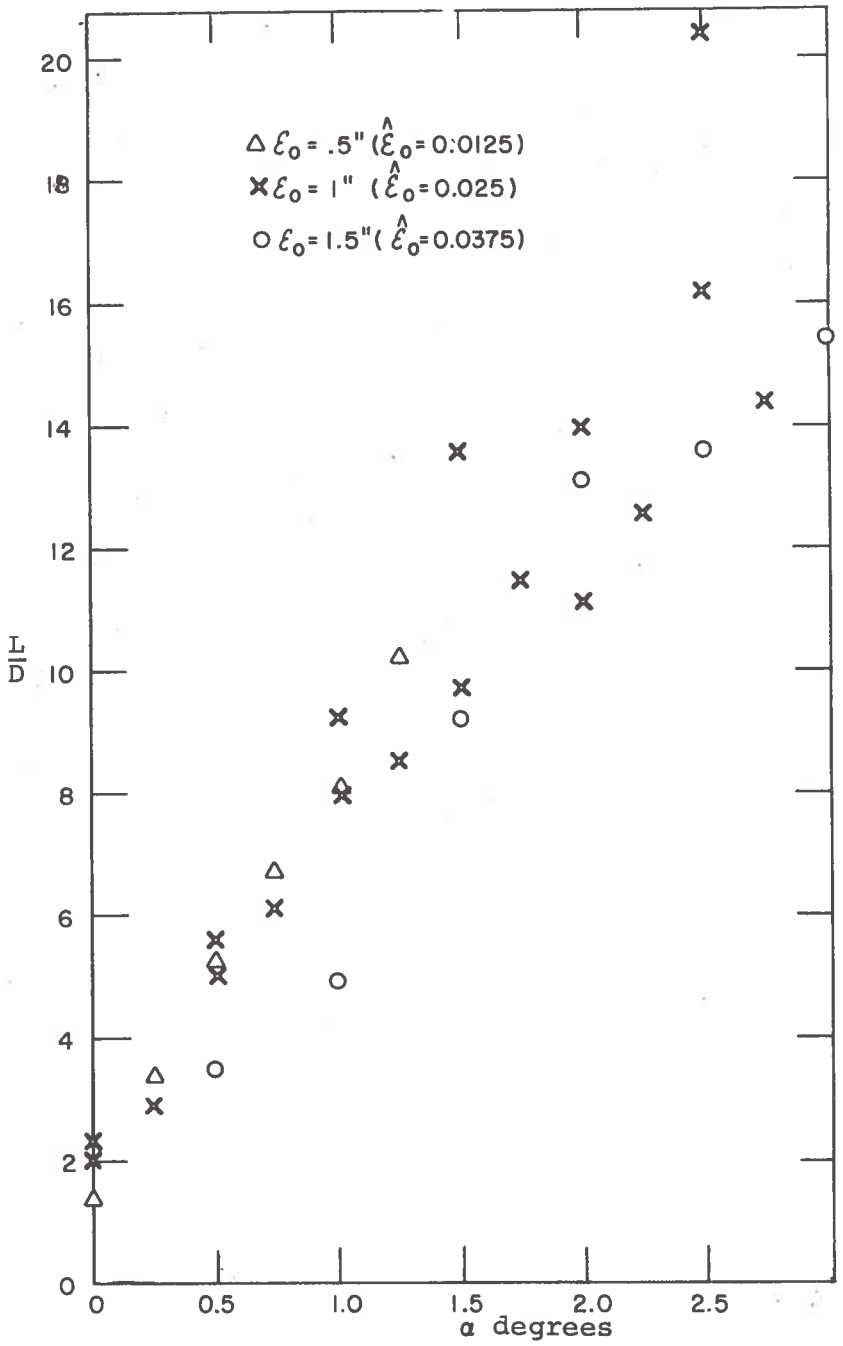

Fig. 14. Lift to drag ratio for $\hat{\delta}_0$ = 0.027

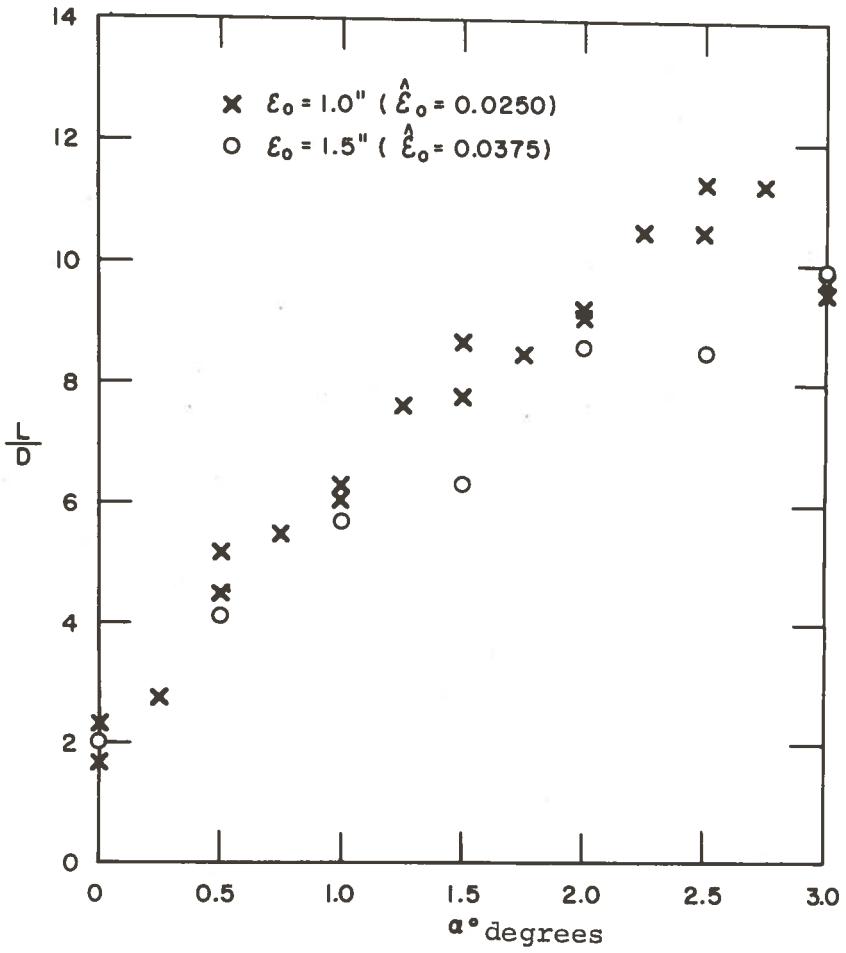

Fig. 15. Lift to drag ratio for $\hat{\delta}_o = 0.04$

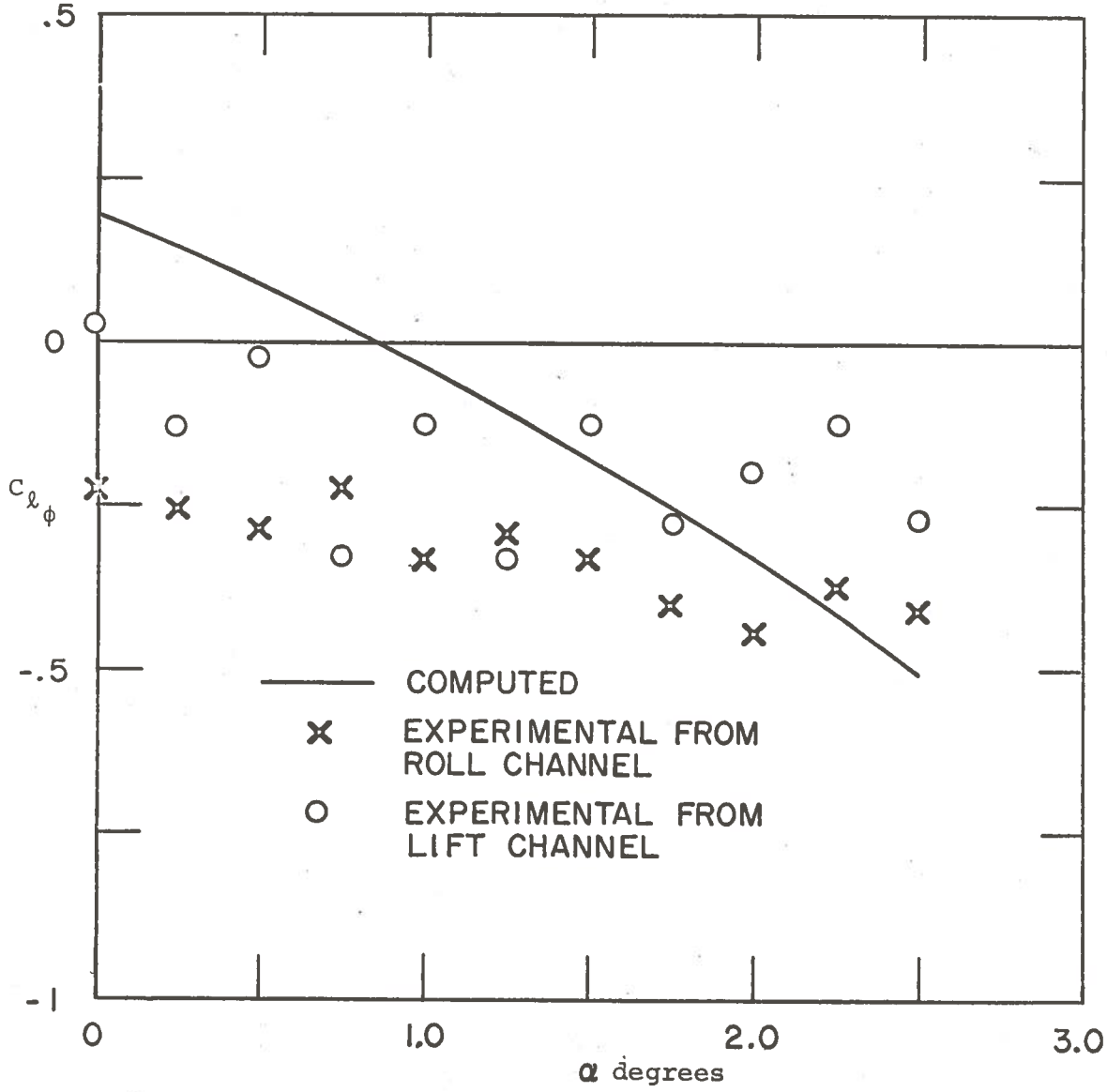

Fig. 16, Rolling moment due to roll coefficient versus angle of attack for $\hat{\delta}_o = 0.027$ and $\hat{\varepsilon}_o = 0.025$

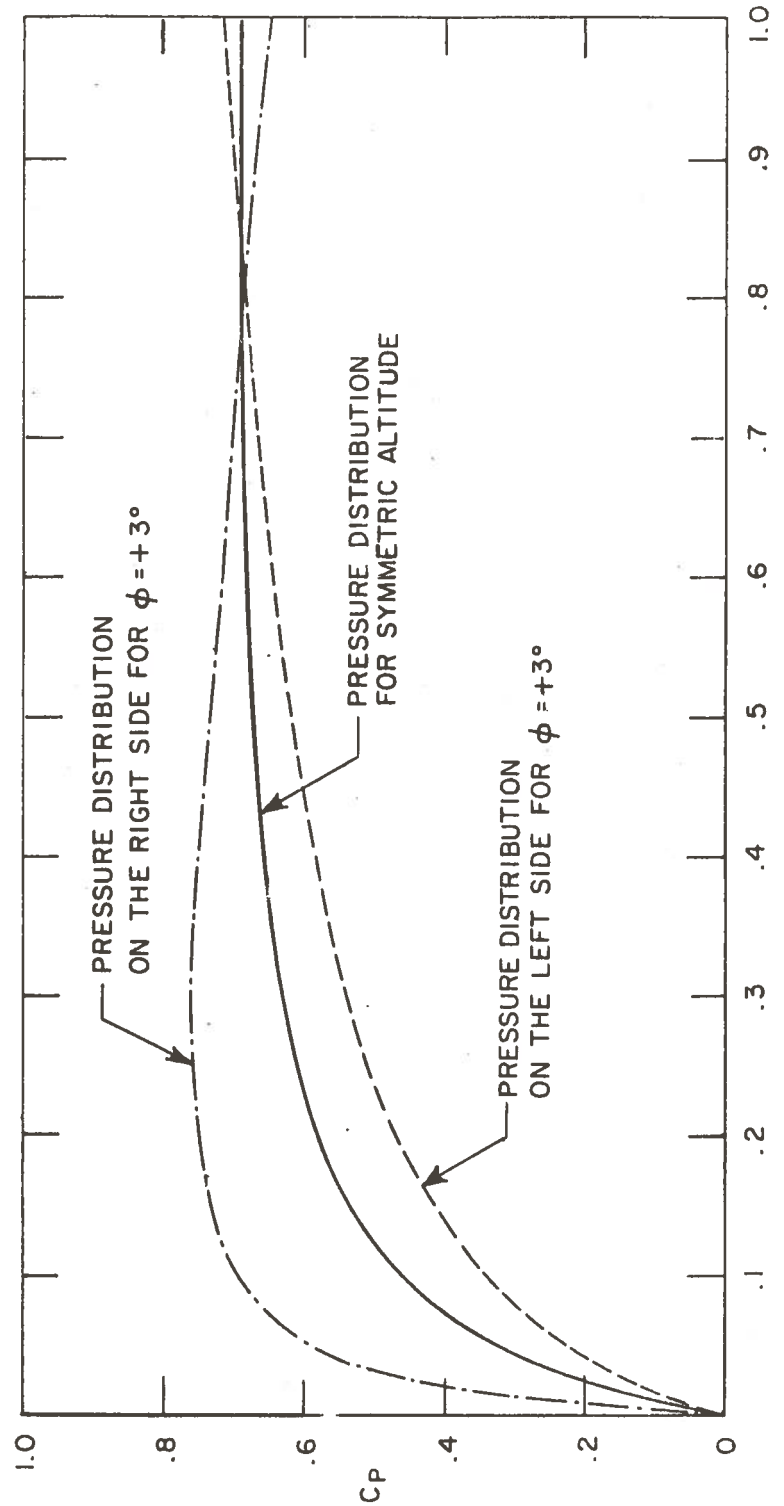

Fig. 17. Computed pressure distribution along chord with and without a roll angle

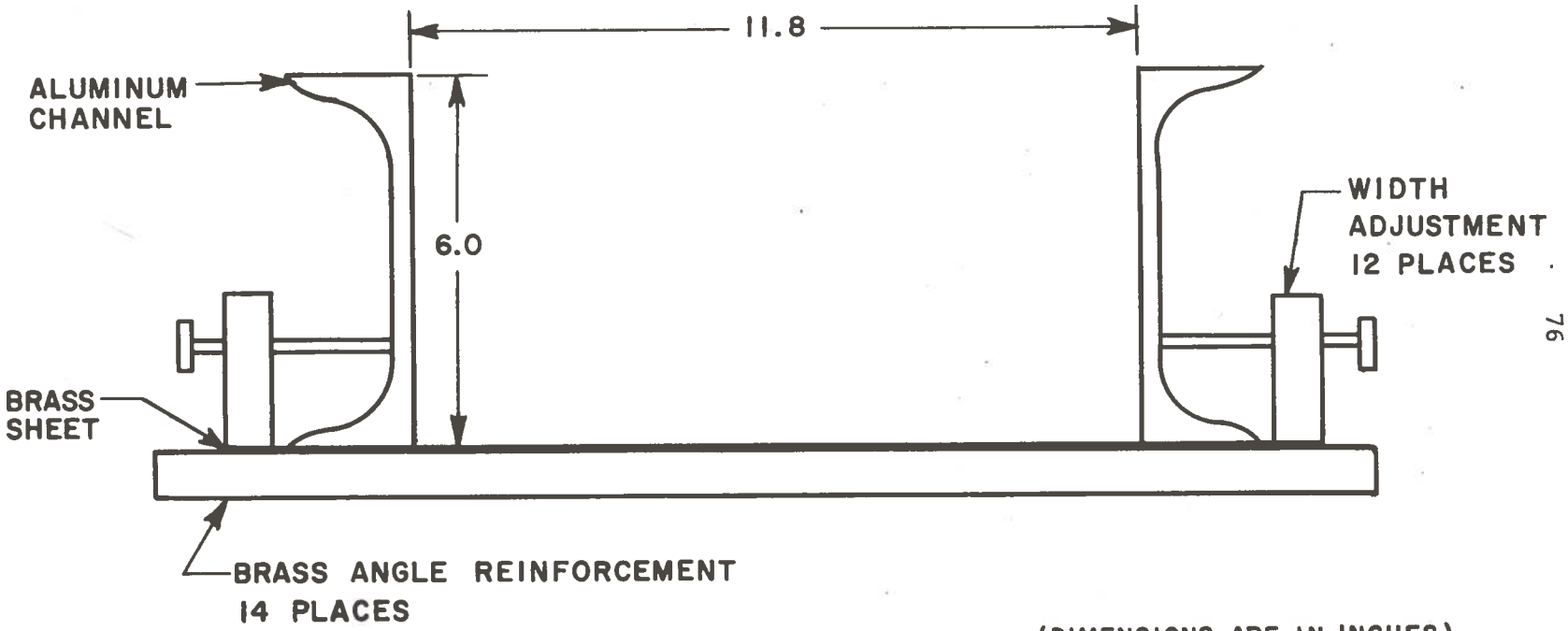

Fig. 18. Schematic Drawing of Guideway Cross-Section

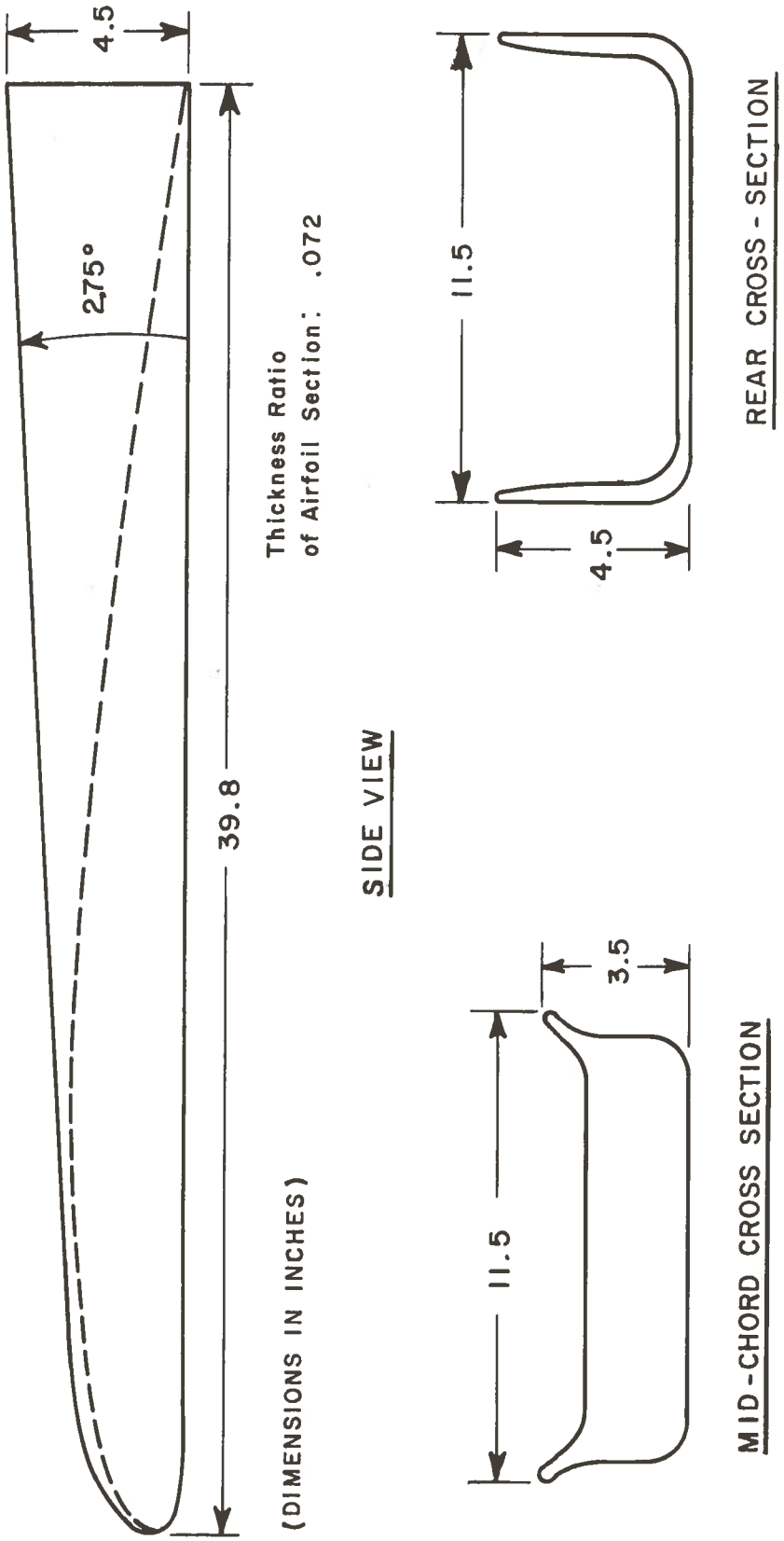

Fig. 19. Schematic Drawing of Model

APPENDIX A

BASIC EQUATIONS OF MOTION

A.1. General Equations

The motion of a ram wing vehicle in a guideway is generally complicated by interactions between it and its guideway. By considering the conservation of linear and angular momentum one can deduce a set of equations whose solution could describe the motion. Considering the state [S] of the vehicle to be described by its coordinates and velocity these equations take the form

$$\frac{d}{dt}\,[S] = [a] \cdot [S] + [F]$$

Here [S] is the "column vector" defined

$$[S] = \begin{pmatrix} \delta_B \\ \phi_B \\ \psi_B \\ V \\ p \\ r \\ h_B \\ w \\ \theta_B \\ q \end{pmatrix} \quad \text{and} \quad [F] = \begin{pmatrix} 0 \\ 0 \\ 0 \\ 0 \\ 0 \\ 0 \\ 0 \\ g \\ 0 \\ 0 \end{pmatrix}$$

Also

$$[a] = \left[\begin{array}{cccccc|cccc} 0 & 0 & 0 & 1 & 0 & 0 & 0 & 0 & 0 & 0 \\ 0 & 0 & 0 & 0 & 1 & 0 & 0 & 0 & 0 & 0 \\ 0 & 0 & 0 & 0 & 0 & 1 & 0 & 0 & 0 & 0 \\ Y_\delta & Y_\phi - g & Y_\psi & Y_v & Y_p & Y_r & Y_h & Y_w & Y_\theta & Y_q \\ L_\delta & L_\phi & L_\psi & L_v & L_p & L_r & L_h & L_w & L_\theta & L_q \\ N_\delta & N_\phi & N_\psi & N_v & N_p & N_r & N_h & N_w & N_\theta & N_q \\ \hline 0 & 0 & 0 & 0 & 0 & 0 & 0 & 1 & 0 & 0 \\ Z_\delta & Z_\phi & Z_\psi & Z_v & Z_p & Z_r & Z_h & Z_w & Z_\theta & Z_q \\ 0 & 0 & 0 & 0 & 0 & 0 & 0 & 0 & 0 & 0 \\ m_\delta & m_\phi & m_\psi & m_v & m_p & m_r & m_h & m_w & m_\theta & m_q \end{array}\right]$$

Note

$$Y_\delta = \frac{1}{m}\frac{\partial Y}{\partial \delta} \text{ etc.}, \quad L_\delta = \frac{\ell_\delta + \frac{E}{A} n_\delta}{1 - \frac{E^2}{A^2}}, \quad N_\delta = \frac{n_\delta + \frac{E}{C}\ell_\delta}{1 - \frac{E^2}{C^2}}$$

$$m_\delta = \frac{1}{I}\frac{\partial M}{\partial \delta}, \quad \ell = \frac{1}{A}\frac{\partial L}{\partial \delta}, \quad n_\delta = \frac{1}{C}\frac{\partial N}{\partial \delta}, \text{ etc.}$$

The [a] matrix has been partitioned so that the longitudinal constant velocity motion (the lower right-hand corner) is separated from the lateral motion (the upper left-hand corner). The cross coupling is caused by the off-diagonal elements. (Note the L_δ and N_δ, etc. contain the inertial cross coupling.) Hence if the off-diagonal elements are zero the lateral and longitudinal motions are uncoupled. If the guideway sides are perpendicular to the guideway floor, and if the ram wing is roughly similar to the guideway, hueristic arguments can be offered that will suggest the coupling is negligible. Note [a] may be a function of [S] so the differential equation is essentially non-linear even though it seems to be in a linear form. Consider some of the coupling terms, in particular the pair y_w

and z_v. It seems reasonable to assume these terms exist in a rectangular guideway only if the vehicle is rolled, even if the vehicle possesses lateral symmetry. However, in a polygonal guideway, these terms will exist as long as $\delta \neq 0$ for any ϕ. Of course these terms are approximately proportional to ϕ or δ. The effect of the coupling can be discussed simply in two limiting cases. First, let all coupling terms vanish save L_h. In this case roll is driven by the pitch-plunge motion. As long as all lateral only eigenvalues are widely separated from the longitudinal only eigenvalues, then the stability is unchanged. However, the pitch-plunge frequencies appear in the lateral motion because of the pitch-plunge forcing function ($L_h \cdot h$). Similarly, the cross coupling may be such that the lateral motion is uncoupled and the longitudinal motion is driven at the (two) lateral frequencies. The implication is that a simple experiment can be devised in which one deliberately separates the longitudinal frequencies from the lateral frequencies and then looks for presence of one in the data of the other.

If one is interested in the stability of motion about trim, it is reasonable to assume small perturbations and also to neglect the control forces and moments. Naturally, if the ram wing requires an automatic controller, these latter forces and moments, as well as the controller dynamics, are needed to study system stability.

A.2 General Linearized Lateral Equations

The basic equations for the lateral motion may be derived

from the upper left partition, that is the variables δ_B, ϕ_B, ψ_B, v, p and r. It is convenient in this particular case to use a coordinate system fixed in the guideway, although the origin is fixed at the center of mass of the vehicle. The vehicle or body axis possesses Euler angles ψ, in yaw, θ in pitch, and ϕ in roll. The vehicle position is determined by yawing, pitching and rolling, IN THAT ORDER. If the body fixed linear velocities are U, V and W, then

$$\frac{d\delta}{dt}=U\cos\theta\sin\psi+V(\sin\phi\sin\theta\sin\psi+\cos\psi\cos\phi)+W(\cos\phi\sin\theta\sin\psi-\sin\phi\cos\psi)$$

For small angles keeping only the first order terms this becomes:

$$\frac{d\delta}{dt} = U_o\psi + v \qquad \text{also } \dot{v} = \ddot{\delta} - U_o\dot{\psi}$$

In the nondimensional form this also writes:

$$D\hat{\delta} = \beta + \psi$$

p and r are related to ϕ and ψ in the following way:

$$p + r\tan\theta - \dot{\phi} = 0$$

$$r\sec\theta - \dot{\psi} = 0$$

If the equilibrium flight is considered to be horizontal or if θ is very small then:

$$p = \dot{\phi}$$

$$r = \dot{\psi}$$

Using this assumption and neglecting acceleration terms such as Y or L the linear force and moment become:

$$\Delta Y = Y_\delta\delta + Y_{\dot{\delta}}\dot{\delta} + Y_\phi\phi + Y_{\dot{\phi}}\dot{\phi} + Y_\psi\psi + Y_{\dot{\psi}}\dot{\psi}$$

$$\Delta L = L_\delta\delta + L_{\dot{\delta}}\dot{\delta} + L_\phi\phi + L_{\dot{\phi}}\dot{\phi} + L_\psi\psi + L_{\dot{\psi}}\dot{\psi}$$

$$\Delta N = N_\delta\delta + N_{\dot{\delta}}\dot{\delta} + N_\phi\phi + N_{\dot{\phi}}\dot{\phi} + N_\psi\psi + N_{\dot{\psi}}\dot{\psi}$$

Note here the coefficients above differ from those in the [a] matrix in a simple way. These coefficients are evaluated

at equilibrium, and are thus constants. This means the lateral equations are linear and their solution can be found more simply. By combining the small angle results $\dot{v} = \ddot{\delta} - V_o\dot{\psi}$, etc. the six first order equations can be reduced to the three classical lateral equations.

$$\begin{aligned} \Delta Y + mg\phi &= m\ddot{\delta} \\ \Delta L &= A\ddot{\delta} - E\ddot{\psi} \\ \Delta N &= -E\ddot{\phi} + C\ddot{\psi} \end{aligned}$$

Only uncontrolled motion being considered here, terms due to changes in the control surface angles have not been included.

A.3. Nondimensional Equations

Dividing the forces by $1/2\ \rho U_o^2 S$, the moments by $\rho U_o^2 Sl$, and replacing $\frac{d}{dt}$ by $D = \frac{d}{d\hat{t}}$ the equations become nondimensional:

$$(2\mu D^2 - C_{Y_{\dot{\delta}}} D - C_{Y_\delta})\hat{\delta} - (C_{Y_{\dot{\phi}}} D + C_{Y_\phi} + C_{L_0})\phi - C_{Y_{\dot{\psi}}} D + C_{Y_\psi})\psi = 0$$

$$-(C_{\ell_{\dot{\delta}}} D + C_{\ell_\delta})\hat{\delta} + (i_A D^2 - C_{\ell_{\dot{\phi}}} D - C_{\ell_\phi})\phi - (i_E D^2 + C_{\ell_{\dot{\psi}}} D + C_{\ell_\psi})\psi = 0$$

$$-(C_{n_{\dot{\delta}}} D + C_{n_\delta})\hat{\delta} - (i_E D^2 + C_{n_{\dot{\phi}}} D + C_{n_\phi})\phi + (i_C D^2 - C_{n_{\dot{\psi}}} D - C_{n_\psi})\psi = 0$$

The difference with the traditional equations for an aircraft is the introduction of terms due to side position C_{Y_δ}, C_{ℓ_δ}, C_{n_δ}, roll position C_{Y_ϕ}, C_{ℓ_ϕ}, C_{n_ϕ}, and yaw position C_{Y_ψ}, C_{ℓ_ψ}, C_{n_ψ}, that cannot be neglected in the study of ram wings because of the importance of boundary effects.

A.4 Simplified Equations

Let us consider the model that was tested in the glide test of reference 1. It flew without touching the side walls with a

clearance on each side of 1/8 inch. Its length was 50 inches. Thus the maximum yaw angle ψ could not be larger than 0.3°.

The same calculation applied to roll leads to $\phi = 3°$ or ten times larger than ψ.

Moreover we are interested in the first place in designing the optimum cross sections for the model and the track. For this purpose the interaction of yaw can be considered secondary.

It seems then reasonable to start with simplified equations neglecting yaw.

However, it should be noted that this is not fully justified. Even though ψ can be considered much smaller than ϕ, it may be of comparable magnitude with β; therefore in the expression $D\hat{\delta} = \beta + \psi$ it is arbitrary to neglect ψ.

Setting $\psi = 0$ for simplicity, the equations become:

$$(2\mu D^2 - C_{Y_\delta} - C_{Y_{\dot{\delta}}} D)\hat{\delta} - (C_{Y_\phi} + C_{Y_{\dot{\phi}}} D + C_{L_0})\phi = 0$$

$$-(C_{\ell_\delta} + C_{\ell_{\dot{\delta}}} D)\hat{\delta} + (i_A D^2 - C_{\ell_{\dot{\phi}}} D - C_{\ell_\phi})\phi = 0$$

The determinant of the coefficients becomes:

$$a_4 s^4 + a_3 s^3 + a_2 s^2 + a_1 s + a_0$$

$$a_4 = 2\mu i_A$$

$$a_3 = -2\mu C_{\ell_{\dot{\phi}}} - i_A C_{Y_{\dot{\delta}}}$$

$$a_2 = -2\mu C_{\ell_\phi} - i_A C_{Y_\delta} + C_{\ell_{\dot{\phi}}} C_{Y_{\dot{\delta}}} - C_{Y_{\dot{\phi}}} C_{\ell_{\dot{\delta}}}$$

$$a_1 = C_{Y_\delta} C_{\ell_{\dot{\phi}}} + C_{Y_{\dot{\delta}}} C_{\ell_\phi} - (C_{L_o} + C_{Y_\phi}) C_{\ell_{\dot{\delta}}} - C_{\ell_\delta} C_{Y_{\dot{\phi}}}$$

$$a_0 = C_{Y_\delta} C_{\ell_\delta} - (C_{L_o} + C_{Y_\phi}) C_{\ell_\delta}$$

For stability all the a_N must be present and positive. It is reasonable to assume that $C_{\ell_\delta} C_{\ell_\phi} C_{\ell_{\dot\delta}} C_{\ell_{\dot\phi}} C_{Y_\delta} C_{Y_{\dot\delta}} C_{Y_\phi} C_{Y_{\dot\phi}}$ are all negative. C_{L_o} is positive.

Then a_4 and a_3 are always positive.

a_2 can only be negative if the term $C_{Y_{\dot\delta}} C_{\ell_\delta}$ is dominant and this is very unlikely since $C_{\ell_{\dot\delta}}$ is expected to be small.

C_{L_o} might very well be $< |C_{Y_\phi}|$ but since $C_{\ell_{\dot\delta}}$ and C_{ℓ_δ} are probably small, a_0 and a_1 will remain positive.

Therefore all the a_i are expected to be positive under all circumstances which is a very encouraging result. Routh's criterion should also be satisfied, that is:

$$a_1 a_2 a_3 - a_4 a_1^2 - a_0 a_3^2 > 0$$

but it is difficult to get into any further discussion without more feeling for the order of magnitude of each coefficient.

A.5 Longitudinal Equations

These have been derived and discussed in ref. 3. Their simplified version (assuming no velocity perturbation) is reported here using our notation:

$$(2\mu D^2 - C_{Z_{\dot h}} D - C_{Z_h})\hat{h} - (C_{Z_{\dot\theta}} + C_{Z_\theta})\theta = 0$$

$$-(C_{m_{\dot h}} D + C_{m_h})\hat{h} + (i_B D^2 - C_{m_{\dot\theta}} D - C_{m_\theta})\theta = 0$$

Therefore four static derivatives and four dynamic derivatives are necessary to the study of the longitudinal dynamics of ram wings.

A.6 Nonlinear Effects

We have assumed so far that all the perturbations about an equilibrium flight condition were so small that it was possible to separate longitudinal and lateral dynamics. Some experiments (ref. 15) have already shown that the lift coefficient C_{L_o} strongly depends on the height or side position. As far as the latter is concerned we can reasonably assume that the lift gained on one side is lost on the other. Furthermore δ_o is small by design and cannot vary by a large amount. On the contrary h is free to vary considerably and this has been observed (reference 1). If it is so, the variation of some lateral derivatives with height should be taken into account, resulting in a nonlinear set of equations as indicated above.

These nonlinear effects might possibly be more important here than they are for a traditional airplane, resulting in particular in a coupling between roll and height. Some simple experiments using the catapulted model could be conducted to evaluate at least the importance of these nonlinear effects.

However at this stage of the understanding of the ram wing's behavior when an optimum design for the cross section of the track and the model has still to be defined, they can be assumed secondary, and they will not be considered until the linear effects are known in more detail.

A.7 Conclusions

This simple preliminary analysis shows the coefficients that are important and which will have to be estimated or

determined experimentally.

If yaw angle and forward velocity are assumed constant, nine static derivatives and eight dynamic derivatives are necessary to study the general aerodynamics of ram wing vehicles.

APPENDIX B

THE STABILITY DERIVATIVES COMPUTATION PROCEDURE

B.1. Longitudinal Derivatives

C_{L_α} is easily obtained as

$$C_{L_\alpha} = \frac{C_L(d\alpha) - C_{L_o}}{d\alpha}$$

remembering that with our notation when α is varied by $d\alpha$, ε is also varied by $X_o \cdot d\alpha$.

C_{m_α}, C_{L_h} and C_{m_h} are all found in a similar fashion.

B.2. Side Force Derivatives

As explained in Chapter 2 only half the model must be considered to compute the variation in side force.

The elementary side force applied to a length dx of one half of the model is

$$dY = c\, C_p\, \ell_1\, dx$$

$$Y = c \cdot \int_o^1 \ell_1 \cdot C_p\, dx$$

When ℓ is constant along the chord

$$Y = c \cdot \ell_1 \cdot C_L$$

$$C_Y = \frac{Y}{c \cdot b} = \frac{\ell_1}{b} C_L = 1/2 \hat{\ell}_1 \cdot C_L$$

so that

$$C_{Y_\delta} = 2 \cdot \frac{-C_{Y_o} + C_Y(\delta)}{\delta} = \frac{C_L(\delta) - C_{L_o}}{\delta} \cdot \hat{\ell}_1$$

$$C_{Y_\phi} = \hat{\ell}_1 \frac{C_L(\phi) - C_{L_o}}{\phi}$$

$$C_{Y_\psi} = \hat{\ell}_1 \frac{C_L(\psi) - C_{L_o}}{\psi}$$

B.3. Rolling Moment Derivatives

As derived in Chapter 2 for constant ℓ_1

$$\ell = [\frac{b^2 c}{8} + c\,\ell_1(\frac{\ell_1}{2} - G)]C_L$$

$$C_\ell = \frac{\ell}{b^2 c} = \frac{1}{8}\,[1 + \hat{\ell}_1(\hat{\ell}_1 - 2\hat{G})]C_L$$

and

$$C_{\ell_\delta} = 2 \cdot \frac{C_\ell(\delta) - C_\ell(o)}{\delta} = \frac{1}{4}\,[1 + \hat{\ell}_1(\hat{\ell}_1 - 2\hat{G})]\,\frac{C_L(\delta) - C_{L_o}}{\delta}$$

$$C_{\ell_\phi} = \frac{1}{4}[1 + \hat{\ell}_1(\hat{\ell}_1 - 2\hat{G})]\,\frac{C_L(\phi) - C_{L_o}}{\phi}$$

$$C_{\ell_\psi} = \frac{1}{4}[1 + \hat{\ell}_1(\hat{\ell}_1 - 2\hat{G})]\,\frac{C_L(\psi) - C_{L_o}}{\psi}$$

B.4. Yawing Moment Derivative

$$dN = c^2 \, C_p (x - x_o) \, dx \, \ell_1$$

$$C_N = \frac{N}{cb^2} = \frac{\ell_1 c}{b^2} \int (x - x_o) \, C_p dx = \frac{1}{2} \frac{\ell_1}{AR} \, C_M$$

$$C_{N_\delta} = \frac{\ell_1}{AR} \, \frac{C_M(\delta) - C_{M_o}}{\delta}$$

$$C_{N_\phi} = \frac{\ell_1}{AR} \, \frac{C_M(\phi) - C_{M_o}}{\phi}$$

$$C_{N_\psi} = \frac{\ell_1}{AR} \, \frac{C_M(\psi) - C_{M_o}}{\psi}$$

APPENDIX C

SOME CONSIDERATIONS ON A RAM WING LATERAL CONTROL SYSTEM

C.1. General Concept

One of the main advantages of ram wing vehicles is their basic stability which is provided by wall effects. Thus the only dynamic problem one has to solve before the operational stage is that of a "smooth" ride. It might turn out to be more efficient to optimize the shape of the vehicle on an aerodynamic or structural basis and to obtain the required damping by means of a control system. In this appendix we want to demonstrate that lateral control could be achieved at a minimum cost.

Our control members will be the "lips" of the vehicle. By moving one of the lips outward, the side gap is decreased and thus provides an opposite side force and rolling moment. To preserve symmetry the left and right lips are moved in the same direction by the same amount.

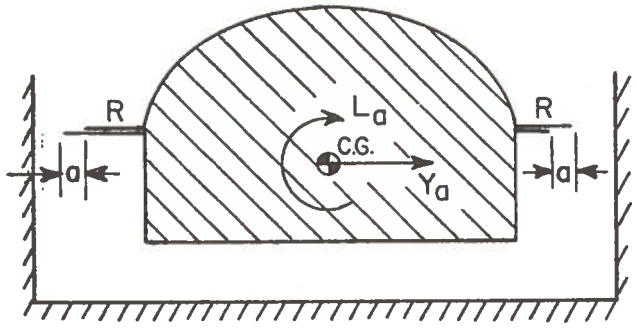

It is noted that the same control system could be used to control the longitudinal motions by moving the lips in opposite directions (which would increase or decrease the lift) or unevenly along the chord (providing more or less pitching moment).

However, if this is done, no additional coupling would be created by the control system which might make its design much easier.

C.2. General Equations

Since the yawing motion is going to be small we can use the simplified lateral equations derived in Appendix A.

Moreover, we shall not consider the dynamic derivatives such as C_{y_δ}, C_{y_ϕ}, etc. ... This amounts to neglecting all natural damping, i.e. to placing ourselves in a worse case than in real life. This is certainly acceptable considering the scope of the following derivations. The resulting equation is:

$$\begin{bmatrix} 2\mu\lambda^2 - C_{y_\delta} & -(C_{y_\phi} + C_{L_o}) \\ -C_{\ell_\delta} & i_A\lambda^2 - C_{\ell_\phi} \end{bmatrix} \begin{bmatrix} \hat{\ell} \\ \phi \end{bmatrix} = \begin{bmatrix} C_{y_a} \\ C_{\ell_a} \end{bmatrix} a$$

To close the loop we need a sensor which will measure either the roll angle (or rate) or the lateral position. Gyros or fluidic systems can give roll very accurately and this is what we shall consider here

$$a = C_1(\lambda)\ \phi$$

$C_1(\lambda)$ is a compensation (which includes the actuator sensitivity).

Since the side gap δ_o is very small we shall assume that a is much smaller than R.

If this is so, moving the lips by a has the same effect as moving the vehicle by a as far as forces and moments are concerned.

Therefore

$$C_{y_\delta} = C_{y_a}$$

$$C_{\ell_\delta} = C_{\ell_a}$$

Gathering everything we have now a new vehicle governed by the following equations

$$\begin{bmatrix} 2\mu\lambda^2 - C_{y_\delta} & -(C_{y_\phi} + C_{L_o}) - C_{y_\delta}C_1(\lambda) \\ -C_{\ell_\delta} & i_A\lambda^2 - C_{\ell_\phi} - C_{\ell_\delta}C_1(\lambda) \end{bmatrix} \begin{bmatrix} \delta \\ \phi \end{bmatrix} = 0$$

The characteristic equation has become:

$$\Delta = \Delta_o - 2\mu\lambda^2 \, C_1(\lambda) \, C_{\ell_\delta} = 0$$

where Δ_o is the free vehicle characteristic equation.

We can study the new dynamics by using the "root locus" technique, the gain being the sensitivity of the actuator and the amplification ratio.

C.3. Some Possible Compensations

C.3.1. $C_1(\lambda) = \frac{-|s|}{2\mu C_{\ell_\delta}}$

$$\Delta + |s| \, \lambda^2 = 0$$

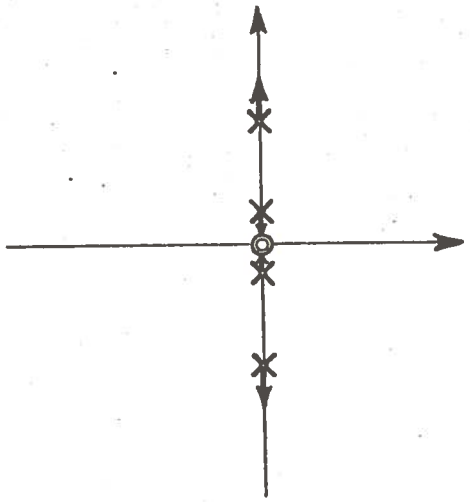

This is not satisfactory.

C.3.2. $C_1(\lambda) = \dfrac{-|S|}{2\mu C_{\ell_\delta}} \lambda$

$$\Delta + |S|\lambda^3 = 0$$

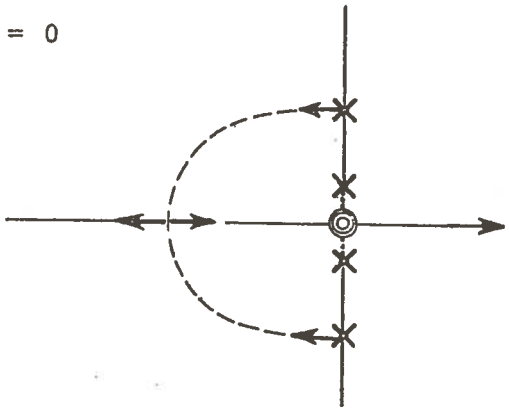

This very simple solution only requires a rate gyro and no compensation. Although it does not seem to be ideal, it must be remembered that some natural damping will be present in the real system so that the root locus would look more like:

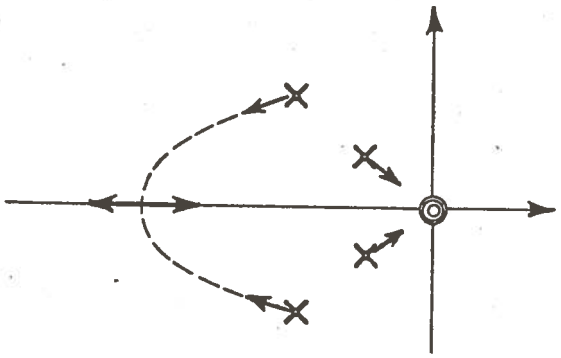

This can probably lead to a satisfactory behavior and it has the advantage of simplicity.

C.3.3. $C_1(\lambda) = \frac{-|S|}{2\mu C_{\ell_\delta}} (\lambda + a_1)$

$$\Delta + |S|(\lambda + a_1)\lambda^2 = 0$$

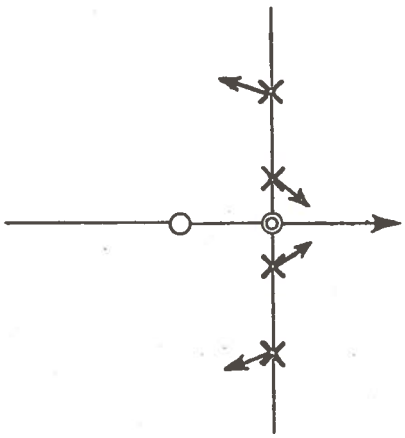

This solution might also become satisfactory when the natural damping is included but it does not seem to offer any advantage over the previous arrangement.

C.3.4. $C_1(\lambda) = \frac{-|S|}{2\mu C_{\ell_\delta}} (\lambda + a_1) \frac{\lambda + a_2}{\lambda + a_3}$

This adds another pole and another zero.

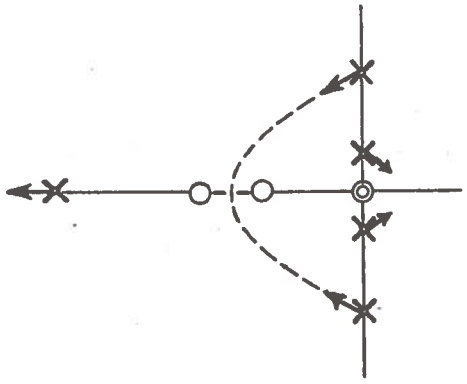

This solution would be appealing because it is very efficient on the higher mode. Unfortunately the lower mode becomes unstable and thus does not improve very much when damping is included.

Decreasing a_3 does not improve the situation until $a_3 = 0$.

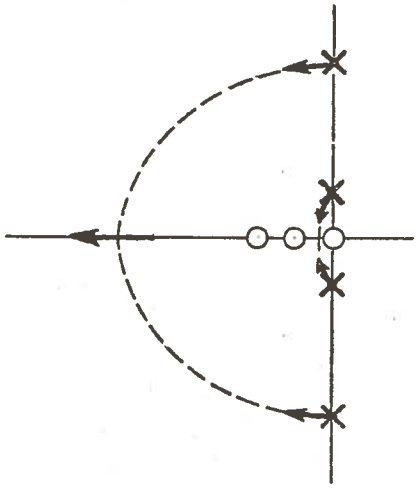

$$\Delta - |S| \lambda (\lambda + a_1)(\lambda + a_2) = 0$$

This last case can be considered very satisfactory and the compensation should not be the cause of any problem.

C.4. Behavior During Turns

As it is the system will tend to keep the vehicle horizontal. However, good comfort will only be obtained if during turns the vehicle is at a certain roll angle so as to keep the specific force perpendicular to the floor.

Since the vehicle has a small aspect ratio and will fly in a track with side wall, the curvature will have to be reduced subsequently. We can therefore assume that all turns will have a comparable radius of curvature so that a roll angle ϕ_o can be defined for turns. When turning begins the control system is sent an input command ϕ_s.

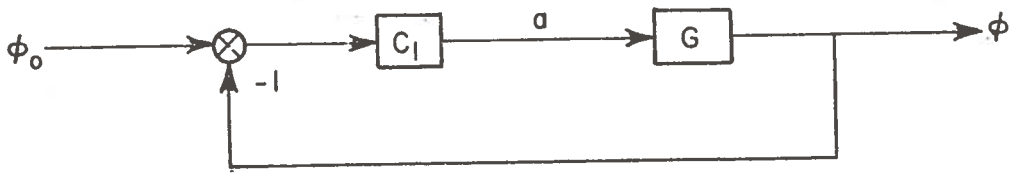

(C_1 being defined here with opposite sign)

$$G = \frac{\phi}{a} = \frac{2\mu C_{\ell_\delta} \lambda^2}{\Delta}$$

$$\frac{\phi}{\phi_o} = \frac{C_1 G}{1+C_1 G} = \frac{2\mu C_{\ell_\delta} \lambda^2 C_1}{\Delta + C_1 \mu C_{\ell_\delta} \lambda^2 \cdot 2}$$

The denominator is the same as studied before so that ϕ_o can be maintained as well as ℓ_o.

C.5. Response to Gust

A gust that would schematically result in a step input or an impulse in ϕ would die out to zero with no oscillation.

APPENDIX D

ANALYSIS OF A POSSIBLE RAM WING CONFIGURATION

D.1. General

Although the model and guideway described in this report were used mainly for reasons of simplicity, it was recognized that their combination was far from ideal. The main problems with this configuration are first, the requirement for an accurate and thus expensive guideway and second, an insufficient stiffness in both height and roll. This appendix therefore contains some preliminary investigation on the following alternative cross section:

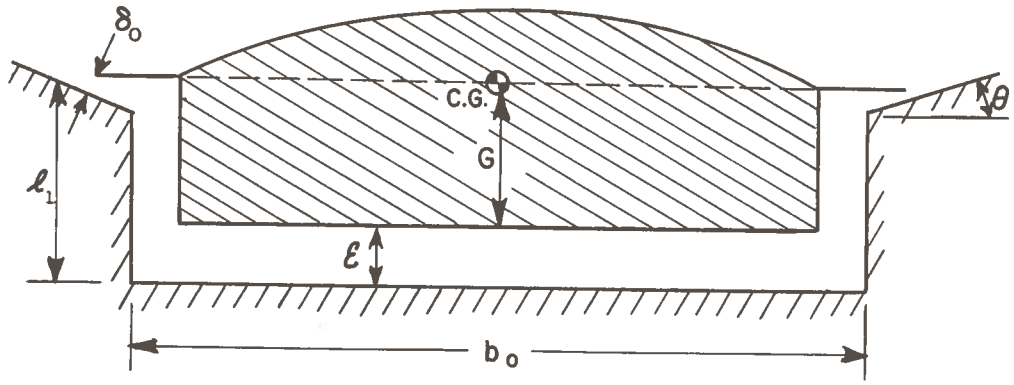

The side gap δ controls the flow the same way as it did before; however, variations in height now result in variations of the side gap which should improve the stiffness greatly. The angle δ can be adjusted so that both stiffness in roll and side force are acceptable. For $\theta = 90°$ we are back to our previous configuration, whereas for $\theta = 0°$ the stiffness in side position would be very close to zero. The same basic modeling of the flow described in Chapter 2 applies again here.

D.2. Derivation of the Equations

Using the same notations as in Chapter 2 the governing equation is again

$$U'(x) = \frac{\hat{H} \cdot \sqrt{1 - U^2(x)} - U(x)\ \hat{A}'}{\hat{A}}$$

except that now

$$\hat{H} = 1/2 \cdot AR \cdot (\hat{\delta}_o - \hat{\delta}\sin\theta - \phi\cos\theta)$$

$$\hat{A} = 1/2\ AR^2\ \hat{\ell}_1(1 - \hat{b}_1) + B\cdot\hat{x}\cdot(\hat{\ell}_1\cdot AR - 2\hat{\varepsilon}) + AR \cdot \hat{\varepsilon} \cdot \hat{b}_1$$

$$- 1/2\ AR^2\ \hat{\ell}_1\ \hat{\delta} - \phi \cdot [\frac{3}{2}\hat{\varepsilon}^2 - \varepsilon\cdot\ell_1\cdot AR + \frac{1}{8} AR^2(1 + \hat{\ell}_1^2)]$$

$$\hat{A}' = AR \cdot \alpha \cdot \hat{b}_1 + B \cdot \hat{\ell}_1 \cdot AR - 2B \cdot (\hat{\varepsilon} + \alpha x)$$

with

$$\hat{\varepsilon} = \hat{\varepsilon}_o + \alpha(x - x_o)$$

$$\hat{\ell}_1 = \text{constant} = \frac{\ell_1}{b/2}$$

$$\hat{b}_1 = \frac{b_1}{b} \text{ and } b_1 = \text{trailing edge width}$$

Because b_o is now the width of the guideway, the span of the model becomes a function of side displacement δ and roll angle ϕ:

$$b = b_o - 2\delta + 2G \cdot \phi$$

or

$$b = b_o \, (1 - \hat{\delta} + \hat{G} \cdot \phi)$$

which changes the expression of the following variables:

$$AR \rightarrow AR(1 - \hat{\delta} + \hat{G} \cdot \phi)$$
$$\hat{\ell}_1 \rightarrow \hat{\ell}_1(1 + \hat{\delta} - \hat{G} \cdot \phi)$$
$$\hat{\delta}_o \rightarrow \hat{\delta}_o(1 + \hat{\delta} - \hat{G} \cdot \phi)$$
$$\hat{b}_1 \rightarrow \hat{b}_1(1 + \hat{\delta} - \hat{G} \cdot \phi)$$

If the center of gravity is located in the lip plane $G = \ell_1 - \varepsilon_o$ or $\hat{G} = \hat{\ell}_1 - 2\hat{\varepsilon}_o/AR$ (recalling that ε is nondimensionalized by the chord rather than the semispan).

D.3. Discussion of the Results

Using the same scheme as in Chapter 2 the pressure field and consequently the lift and the stability derivatives can be obtained.

The following values have been retained:

$\hat{\ell}_1 = 2/3$	$\hat{\varepsilon}_o = 0.025$
$\hat{\delta}_o = 0.025$	$\alpha = 0.026$
$\hat{b}_1 = 0.98$	$B = 0.025$
$AR = 0.3$	$X_o = 0.5$

They yield a lift coefficient very close to 0.5.

The lateral derivatives can now be computed as a function of the angle θ. The results are plotted in Fig. D-1.

As expected, the values of the four stability derivatives considered here vary essentially as either sin θ or cos θ. Moreover C_{y_δ} and C_{ℓ_δ} are close to being symmetrical to C_{y_ϕ} and C_{ℓ_ϕ} respectively. This demonstrates again that the primary effect in the presence of side displacement or roll is that of side gap closure or opening. The value $\theta = 45°$ is therefore the one that gives the best combination of side and roll stiffness. It should be noted that the roll stiffness can also be improved by lowering the center of gravity. However, to keep the cost of the guideway as low as possible the height ℓ_1 is expected to be small compared to b_o (here 1/3) and therefore an angle $\theta \neq 90°$ is indeed useful. If the two effects are combined, the best angle θ is about 50° or 55°.

The stiffness in height versus θ is plotted in Fig. D-2. This stiffness is multiplied by four when $\theta = 45°$.

D.4. Conclusions

This preliminary investigation is a good example of how our simplified mathematical model can be used for preliminary design purposes. The new configuration considered has improved stiffness and probably requires a cheaper guideway; the best side angle is as expected, around 45 degrees. One of its disadvantages might be a greater sensitivity to cross winds.

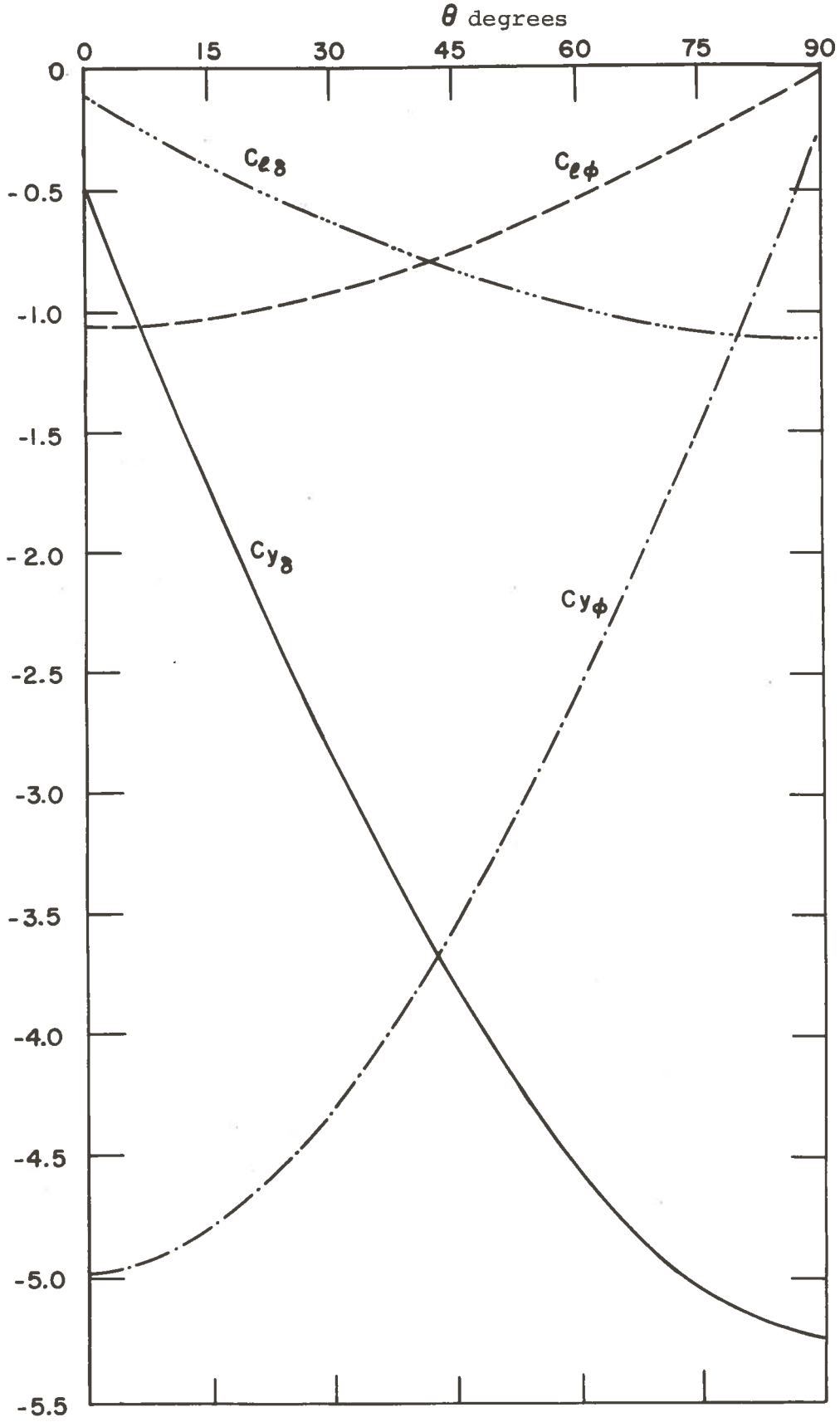

Fig. D-1. C_{y_δ}, C_{y_ϕ}, C_{ℓ_δ} and C_{ℓ_ϕ} versus θ

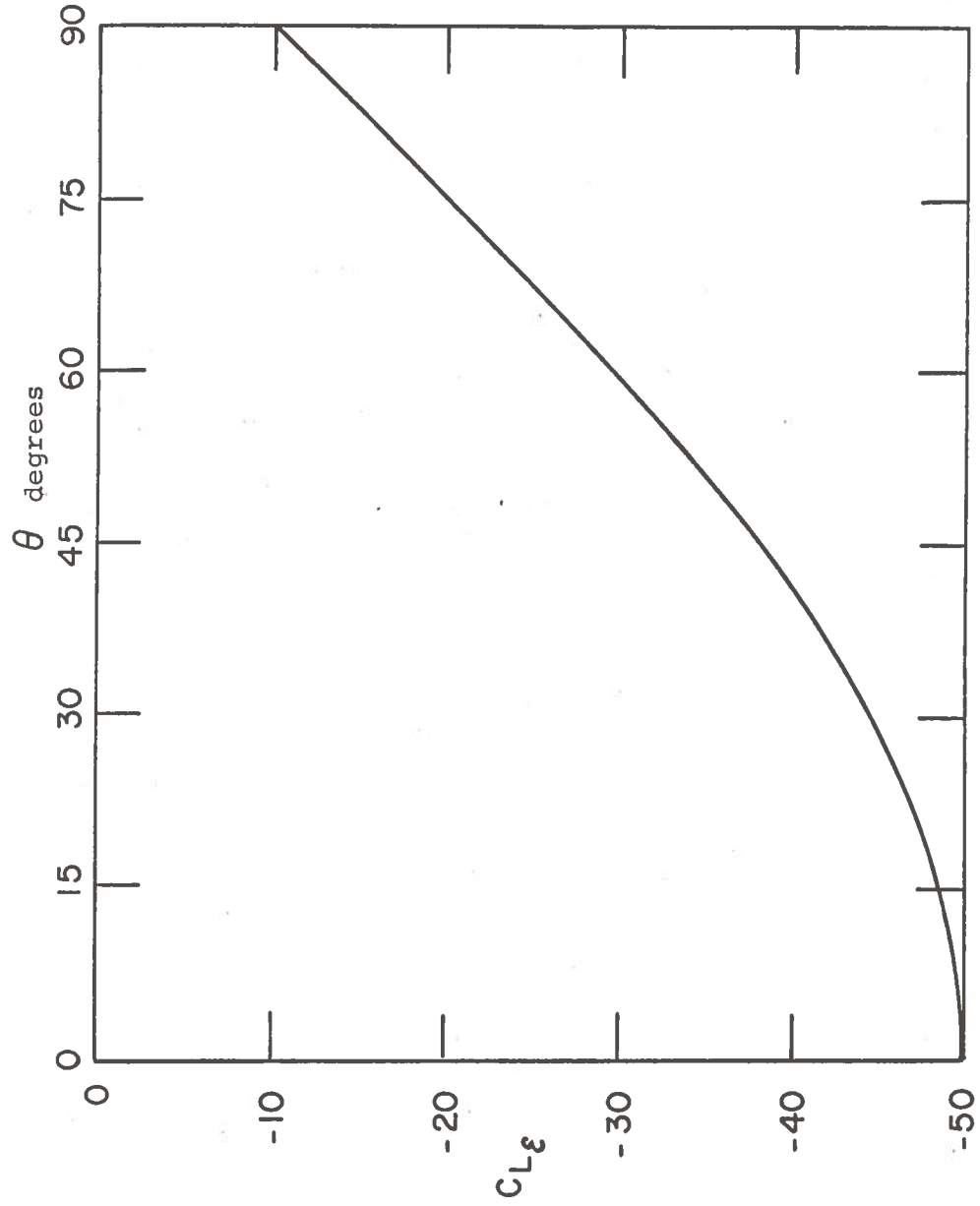

D-2. Variation in lift due to height variation coefficient versus angle of θ

APPENDIX E

REPORT OF INVENTIONS

After diligent review of the work performed under this contract (DOT-TSC-239), no new innovation, discovery, improvement or invention was made.

REFERENCES

1. Barrows, T. M., "Progress on the Ram Wing Concept with Emphasis on Lateral Dynamics," Accession No. PB210743.

2. Gallington, Miller and Smith, "The Ram Wing Surface Effect Vehicle," Hovering Craft and Hydrofoil, Vol 11, No. 5, February 1972.

3. Barrows, T. M., "The Use of Aerodynamic Lift for Application to High Speed Ground Transportation," Prepared for D.O.T., Accession No. PB 197 242.

4. Lippisch, A., "The Principles of Ground Effect and the Development of the Aerofoil Boat," Liftfahrttechnik Raumfahrttechnik, October 1964.

6. --- "Proceedings of the Symposium on the Towing Tank Facility Instrumentation and Measuring Technique," edit. V. A. Sentic, Zagreb, 1960.

7. Turner, T. R., "Endless Belt Technique for Ground Simulation," NASA SP 116, 1966.

8. Vogler, R. D., "Ground Effects on ... VTOL Models... Over Stationary and Moving Ground Planes," NASA TN D 3213 1966.

9. Turner, T. R., "A Moving Belt Ground Plane for Wind Tunnel Ground Simulation," NASA TN D 3228, 1967.

10. Turner, T. R., "Wind Tunnel Investigation of a 3/8 Scale Automobile Model Over a Moving Belt Ground Plane," NASA TN D 3229, 1967.

11. Halliday, A. S., "The New Whirling Arm at the National Physical Laboratory," ARC TR RM No. 2286.

12. Kumar, P. E., "The College of Aeronautics Whirling Arm Initial Development Tests," COA Note Aero. No. 174.

13. Ashill, P. R., "Calibration of the Flow in the Channel of the Whirling Arm," COA Note No. 177.

REFERENCES (continued)

14. Holloway, W. G., "Development of a Three-Component Strain Gauge for Use on the Whirling Arm," COA Note No. 178.

15. Pepin, J. N., "Study of a Ram Wing in a Trough," M.I.T. MS thesis, 1970.

16. Goodson, K. W., "Effect of Ground Proximity of the Longitudinal Lateral and Control Aerodynamic Characteristics of a V/STOL Model," NASA TN D 3237, 1967.

17. Kumar, P. E., "Stability of Ground Effect Wings," COA Report No. 196.

18. Kumar, P. E., "An Experimental Investigation into the Aerodynamic Characteristics of the Wing in Ground Effect," COA Report No. 201.

19. Kumar, P. E., "On the Longitudinal Dynamic Stability of A Ground Effect Wing," COA Report No. 202.

20. Kumar, P. E., "The Lateral Dynamics of a Ground Effect Wing," COA Report No. 207.

21. Wollard, H. W., and Sergeant, R. J., "An Experimental Investigation of the Hover and Forward Speed Aerodynamic Characteristics of Several Tracked Air Cushion Vehicle Models," AIAA paper No. 69-750.

22. Boccadoro, Y. A., "Contribution to the Study of a Flat Bottomed Ram Wing Vehicle," M.I.T. MS/EAA thesis, 1972.

23. Barrows, T.M., "Analytic Studies of the Lift and Roll Stability of a Ram Air Cushion Vehicle," 1972. Accession No. PB219820

Note: Reports with PB prefixes can be obtained from the National Technical Information Service (NTIS), Springfield, Virginia 22151.